Available online at www.sciencedirect.com
ScienceDirect
Comput. Methods Appl. Mech. Engrg. 373 (2021) 113532
Computer methods in applied mechanics and engineering
www.elsevier.com/locate/cma

An adaptive model order reduction method for boundary element-based multi-frequency acoustic wave problems

Xiang Xie*, Yijun Liu

Department of Mechanics and Aerospace Engineering, Southern University of Science and Technology, Shenzhen, 518055, China

Received 27 June 2020; received in revised form 19 October 2020; accepted 20 October 2020
Available online 7 November 2020

Abstract

The classical boundary element method (BEM) is widely used to obtain detailed information on the acoustic performance of large-scale dynamical systems due to the nature of semi-analytical characteristic. Its use, however, results in asymmetric and dense system matrix, which makes original full-order model evaluation very time consuming and memory demanding. Moreover, the frequency sweep analysis which is indispensable for the assessment of noise emission levels and the design of high-quality products requires the repetitive assembly and solution of system of equations, which further increases the computational complexity. In order to alleviate these problems, an adaptive structure-preserving model order reduction method is presented, which is based on an offline–online solution framework. In the offline phase, we first factor out the frequency term as a scalar function from the BE integral kernels of the Burton–Miller formulation, followed by integration to set up the system matrices. A global frequency-independent orthonormal basis is then constructed via the second-order Arnoldi (SOAR) method to span a projection subspace, onto which the frequency-decoupled system matrices are projected column by column to solve the memory problem arising from the frequency-related decomposition. In addition, the number of iterations required for convergence can be automatically determined by exploiting the condition number of an upper Hessenberg matrix in SOAR. In the online stage, a reliable reduced-order model can be quickly recovered by the sum of those offline stored reduced matrices multiplied by frequency-dependent coefficients, which is favored in many-query applications. Two academic benchmarks and a more realistic problem are investigated in order to demonstrate the potentials of the proposed approach.

Keywords: Boundary element method; Adaptive model order reduction; Burton–Miller formulation; Second-order Arnoldi; Frequency sweep

1. Introduction

Over the past years, the acoustic qualities of dynamical systems have become an important design criterion in many industrial sectors, for instance, high-speed trains, automobiles, aircraft fuselages, etc. Therefore, fast and efficient modeling of acoustic fields is highly desirable for the noise control and low-noise design. Among the various computational methods, the finite element method (FEM) [1] and boundary element method (BEM) [2] are of special interest to facilitate numerical simulations of structural acoustic problems. Compared with the FEM, the BEM might be preferable to handle three-dimensional (3D) exterior acoustic computations because of its inherent advantages such as decreasing the dimension of involved problems from 3D to 2D and satisfying the far-field

* Corresponding author.
E-mail addresses: xiex@sustech.edu.cn (X. Xie), liuyj3@sustech.edu.cn (Y.J. Liu).

https://doi.org/10.1016/j.cma.2020.113532
0045-7825/

boundary condition (BC) exactly. One of the weaknesses in the conventional BEM for exterior acoustic problems is the existence of non-unique solutions. The combined Helmholtz integral equation formulation (CHIEF) has been proposed to avoid this difficulty [3]. However, there are no analytical rules to guide how to choose the number and position of interior points for the derivation of the over-determined system of equations. The Burton–Miller boundary integral equation (BIE) formulation [4] is another way to deal with this problem and has proven to be more rigorous and popular [5,6].

In addition, the coefficient matrix of BEM is fully populated and nonsymmetric, which leads to excessive memory usage and calculation time. The fast multipole boundary element method [7,8] which is based on the separation of field and source points in the Green's function has been proposed to improve the efficiency of solving large-scale problems. For acoustic modal analysis with BEM, the dual and multiple reciprocity method [9,10], contour integral method [11] and resolvent sampling based Rayleigh–Ritz method [12] have been employed to compute the related nonlinear eigenvalue problem. In practice, the frequency spectra of excitation generally have a broad frequency band and thus multi-frequency analysis is often required. Because of the frequency-dependent property, both the traditional BEM and fast multipole BEM have to be applied to intensively recalculate all the entries in the system matrices and then resolve it at multiple frequencies. As a result, the direct system-level simulation of the original BE model over a wide frequency range is extremely prohibitive. Therefore, there is a strong need for efficient computational approaches, capable of predicting the acoustic radiation and scattering properties of increasingly complex systems at low cost.

A logical strategy to overcome the drawback is to eliminate the frequency dependency, which has been explored by using various forms of expansions of the kernels [13–15], including but not limited to the Taylor series. Such an approach reduces the integration effort for assembling the coefficient matrix, while the memory problem becomes however more serious. This is a common trade-off between the computational speed and memory consumption. The empirical interpolation method can also be used to decouple the frequency from the Green's function as reported in [16] for parameter-dependent cases.

Another alternative way to circumvent the difficulty incurred by acoustic frequency sweeps is to use model order reduction (MOR) methods, which attempt to construct a low-order approximation of the original system to reduce the overall computational burden of numerical simulations. Though extensive literature exists on MOR methods, however, the dimension reduction of BE models has received less attention than that of FE models [17]. The main challenges in reducing BE systems are two-fold: (1) how to construct an orthonormal basis and (2) how to avoid the assembly of system matrices for each frequency before projection. Some frequency interpolation techniques such as the padé approximant have been used to extrapolate the acoustic transfer functions of BE models between a number of selected master frequencies [18–20]. The proper orthogonal decomposition (POD) technique can be applied to linear as well as nonlinear systems, thus it can naturally be used to speed up the solution of BE models [21,22]. In these approaches, the quality of approximation heavily depends on the selection of samples (e.g. through the use of greedy algorithm [23]), and also multiple high-fidelity evaluations for snapshots (or master frequencies) are necessary, which are undesirable in many practical applications. Reduction of the dimension of system of equations comes down to identify a proper projection subspace onto which the full-order model (FOM) can be projected to establish a compact reduced-order model (ROM). A family of the most effective methods in the moment matching research community is based on the construction of the Krylov subspace [24–26]. Such an iterative approach which takes the advantages of simplicity, availability and fast convergence has been used for reduced-order modeling of BE systems [21,27]. All of the aforementioned methods proposed in the literature can be directly applied to construct an orthonormal basis for BE models without any difficulty, which responds the first challenge. However, the projection step is rather troublesome because it requires first forming the underlying FOM at each new value of the frequency, then projecting this model onto the reduced-order basis. This way, the ROM constructed for capturing the dynamic behavior of original FOM is updated successively as frequency varies, which is less favorable.

Following the first author's previous work for dimension reduction of FE dynamical systems with frequency-dependent damping [28,29], we first introduce a transformation based on Taylor's theorem to treat the frequency-dependent Green's function. After that, MOR techniques can be applied to the frequency-decoupled system matrices to ease the computational complexity. This idea enjoys the combination of both strengths of the series expansions and the MOR methods, which recently has been adopted in [30] to find a representative basis for BE systems with the CHIEF method. In this work, a completely distinct and superior model reduction approach which is based on the second-order Arnoldi (SOAR) algorithm [31] is developed for dimension reduction of large-scale BE models with the Burton–Miller formulation to remove the fictitious eigenfrequency difficulty.

Since obtaining better approximation and smaller model size are the goals in the model reduction process, an important open question is how to determine the order of a reduced model with satisfactory accuracy for practical use, preferably in an adaptive manner. The strategies proposed in the literature for FE models are often based on the relative input/output residual [23,24,32] or the difference between two reduced-order models [24,33–35] to estimate the true error such that the evaluation of the FOM can be avoided. Considering computational resource limitations, application of these adaptive strategies is not a big problem for sparse FE matrices, but for dense BE matrices, numerical difficulties arise. This is because the system matrices need to be explicitly assembled and stored. Meanwhile, it also implies that multiple projections of the FOM onto different low-dimensional subspaces and solution of the different reduced models are necessary to compare and check each other's accuracy until a prescribed threshold is satisfied, as conducted in [30]. Obviously, the frequent comparisons are quite expensive. Therefore, it is preferred that the number of moments matched between the BE FOM and its low-order approximation can be determined before the model reduction process starts not as the model reduction evolves.

To achieve this, an adaptive scheme which is based on the condition number of an upper Hessenberg matrix is incorporated into the SOAR process to automatically determine the desired low order. This provides a simple yet powerful tool for engineering many-query applications, such as evaluation of a BE model many times for multi-frequency analyses. We refer to the proposed procedure for the construction of frequency-independent approximation basis as the Adaptive Taylor-based SOAR (AT-SOAR) approach [29] from now on. At the end of the offline phase, a column-by-column projection is performed without even forming the system matrices explicitly and the resulting reduced matrices/vectors are stored for the subsequent fast frequency sweep analysis. In the online stage, one only needs to do straightforward algebraic manipulation on the ROM with a significantly smaller system size, thereby resulting in far less computational cost. To show the benefits of the AT-SOAR approach from both memory and computation time viewpoints, two academic benchmark models with different BCs and a more complex one are taken into account through the study of their acoustic scattering features.

The remainder of the paper is organized as follows. In Section 2, the Burton–Miller formulation as well as the selection of the coupling parameter is introduced. In Section 3, we show a procedure based on Taylor's theorem and the SOAR algorithm to generate an orthonormal basis for reduced-order modeling of BE systems, where different BCs are reformulated. In Section 4, the proposed adaptive scheme and column-by-column projection are elaborated. Numerical verification cases and detailed discussions are highlighted in Section 5. Conclusions and future work are presented in Section 6.

2. Burton–Miller BIE formulation

The governing equation for steady-state linear acoustics in a bounded or unbounded 3D acoustic domain Ω can be expressed by the Helmholtz equation:

$$\nabla^2 p(\mathbf{x}) + k^2 p(\mathbf{x}) = 0, \quad \forall \mathbf{x} \in \Omega \tag{1}$$

where ∇^2 denotes the Laplacian operator; $p(\mathbf{x})$ is the sound pressure; $k = 2\pi f/c$ is the wavenumber which is directly related to the speed of sound c in the medium and the frequency f in Hz.

On the acoustic problem boundary ($\partial\Omega = \Gamma$), the following quantities may be prescribed

$$\begin{aligned} &\text{Neumann BC} \quad \forall \mathbf{x} \in \Gamma_{\mathrm{v}} : q(\mathbf{x}) = \frac{\partial p(\mathbf{x})}{\partial n(\mathbf{x})} = \mathrm{j}\rho\omega\bar{v}_n(\mathbf{x}), \\ &\text{Dirichlet BC} \quad \forall \mathbf{x} \in \Gamma_{\mathrm{p}} : p(\mathbf{x}) = \bar{p}(\mathbf{x}), \end{aligned} \qquad \Gamma = \Gamma_{\mathrm{v}} \cup \Gamma_{\mathrm{p}} \tag{2}$$

where $q(\mathbf{x})$ is the normal derivative of sound pressure at point $\mathbf{x}$ and n is the normal of the boundary; $\bar{v}_n(\mathbf{x})$ and $\bar{p}(\mathbf{x})$ are the imposed normal velocity and sound pressure; ρ is the mass density of the medium; j is the imaginary unit. For exterior acoustic problems, the Sommerfeld radiation condition at infinity must be met

$$\lim_{R\to\infty}\left[R\left|\frac{\partial p}{\partial R} - \mathrm{j}kp\right|\right] = 0, \tag{3}$$

where R is the distance from the origin. Throughout this work, the harmonic time factor $\mathrm{e}^{-\mathrm{j}\omega t}$ is assumed.

By means of the second Green's identity and the Dirac function property, the transformation of Eq. (1) into the conventional boundary integral equation (CBIE) can be derived as [8]

$$C(\mathbf{x})p(\mathbf{x}) = \int_{\Gamma} [G(\mathbf{x},\mathbf{y})q(\mathbf{y}) - H(\mathbf{x},\mathbf{y})p(\mathbf{y})]\,\mathrm{d}\Gamma(\mathbf{y}) + p^{\mathrm{I}}(\mathbf{x}), \tag{4}$$

in which $C(\mathbf{x}) = 1/2$ if the source point $\mathbf{x} \in \mathbb{R}^3$ is located on a smooth boundary surface Γ; $\mathbf{y} \in \mathbb{R}^3$ indicates the field point; $p^{\mathrm{I}}(\mathbf{x})$ denotes the background incident pressure field for scattering problems and it is non-existent for radiation problems; $G(\mathbf{x}, \mathbf{y})$ is known as the free-space Green's function. For 3D acoustic wave problems, it is given by

$$G(\mathbf{x}, \mathbf{y}) = \frac{\mathrm{e}^{\mathrm{j}kr}}{4\pi r}, \tag{5}$$

where r is the distance between $\mathbf{x}$ and $\mathbf{y}$, i.e. $r = |\mathbf{x} - \mathbf{y}|$ and the normal derivative of the fundamental solution is denoted by

$$H(\mathbf{x}, \mathbf{y}) = \frac{\partial G(\mathbf{x}, \mathbf{y})}{\partial n(\mathbf{y})} = \frac{\mathrm{e}^{\mathrm{j}kr}}{4\pi r^2}(\mathrm{j}kr - 1)\frac{\partial r}{\partial n(\mathbf{y})}. \tag{6}$$

It is well-known that the CBIE in Eq. (4) gives non-unique solutions for exterior acoustic problems at a set of fictitious eigenfrequencies [3]. A common way to fix this issue is to use the Burton–Miller BIE formulation [4,8], which is a linear combination of the CBIE and its normal derivative with respect to the vector $n(\mathbf{x})$ at the surface point $\mathbf{x} \in \Gamma$. In this way, the corresponding hypersingular boundary integral equation (HBIE) can be written as

$$C(\mathbf{x})q(\mathbf{x}) = \int_{\Gamma} [E(\mathbf{x}, \mathbf{y})q(\mathbf{y}) - F(\mathbf{x}, \mathbf{y})p(\mathbf{y})]\, \mathrm{d}\Gamma(\mathbf{y}) + q^{\mathrm{I}}(\mathbf{x}), \tag{7}$$

where $q^{\mathrm{I}}(\mathbf{x})$ is the normal derivative of the incident wave field $p^{\mathrm{I}}(\mathbf{x})$. The two new kernels can be expressed as

$$E(\mathbf{x}, \mathbf{y}) = \frac{\mathrm{e}^{\mathrm{j}kr}}{4\pi r^2}(1 - \mathrm{j}kr)\frac{\partial r}{\partial n(\mathbf{x})}, \tag{8}$$

$$F(\mathbf{x}, \mathbf{y}) = \frac{\mathrm{e}^{\mathrm{j}kr}}{4\pi r^3}\left[(1 - \mathrm{j}kr)n_i(\mathbf{x})n_i(\mathbf{y}) + (k^2r^2 + 3\mathrm{j}kr - 3)\frac{\partial r}{\partial n(\mathbf{x})}\frac{\partial r}{\partial n(\mathbf{y})}\right], \tag{9}$$

where n_i being the Cartesian components of the normal $n(\mathbf{x})$ or $n(\mathbf{y})$. By dividing the boundary Γ using surface elements with nodes, the discretization of Eqs. (4) and (7) results in the following matrix form as:

$$[\mathbf{H} + \beta\mathbf{F}]\mathbf{p} = [\mathbf{G} + \beta\mathbf{E}]\mathbf{q} + \mathbf{b}^{\mathrm{I}}, \tag{10}$$

where $\mathbf{b}^{\mathrm{I}}$ is related to the (known) incident wave; $\mathbf{p}$ and $\mathbf{q}$ are respectively the vectors of sound pressure and its normal derivative. More details concerning this Burton–Miller matrix formulation and its explicit expressions can be referred to the review article [6] and monograph [8]. β is the coupling parameter and should be a complex number with $\mathrm{Im}(\beta) \neq 0$. Usually, $\beta = \mathrm{j}/k$ is suggested [36,37] due to the fact that the $\mathbf{G}$, $\mathbf{H}$ and $\mathbf{E}$, $\mathbf{F}$ in Eq. (10) have different order about wavenumber k. In this work, $\beta = \mathrm{j}h$ is selected, where h is a typical element size in the surface mesh. The reasons, on the one hand, are because of the rule of thumb, which implies that the influence of the wavenumber k (or the frequency f) is correlated with the mesh size. On the other hand, it is because that this choice of the coupling parameter yields BE matrices with better conditioning and more stable results [6].

The Burton–Miller approach, however, endures two major disadvantages; the integral operation for each pair of elements is doubled and, even worse, the evaluation of the hypersingular integral is required. Some methods have been suggested to handle the hypersingular integral [38–41]. In this study, the constant triangular elements are applied, which makes the evaluation of singular and hypersingular integrals in Eqs. (4) and (7) can be performed analytically. However, the following solution framework is independent of the basis function used. That is to say, the proposed approach can also be readily applied to BE systems modeled using other basis functions [42,43], e.g. Lagrangian bases with different orders, NURBS, T-splines and even others.

By applying the BCs in Eq. (2) and rearranging (the unknown and known) terms in Eq. (10) lead to the following linear system of equations

$$\bar{\mathbf{A}}\mathbf{z} = \mathbf{b}, \tag{11}$$

where $\bar{\mathbf{A}} \in \mathbb{C}^{N\times N}$ is the coefficient matrix which is fully populated, asymmetric and frequency-dependent; $\mathbf{z} \in \mathbb{C}^N$ and $\mathbf{b} \in \mathbb{C}^N$ are the unknown and known nodal vectors, respectively. N is the number of degrees of freedom (DOFs) in the BE model. Once $\mathbf{z}$ is obtained by using a direct or iterative solver, together with the specified BCs, Eqs. (4) and (7) with $C(\mathbf{x}) = 1$ can be used to calculate the sound pressure p and normal velocity v_n of any point within the domain Ω, or more generally, the acoustic system output can be given by

$$y = \mathbf{L}^{\mathrm{T}}\mathbf{z}, \tag{12}$$

where $\mathbf{L} \in \mathbb{C}^N$ is usually an output measurement vector to calculate any variable of interest from the BE solution vector (e.g. sound power, sound intensity, etc.). In this work, it is only used to pick certain DOFs. The superscript T designates the transpose operation.

3. MOR for BEM via T-SOAR procedure

It is obvious that the conventional BEM requires $\mathcal{O}(N^2)$ operations to calculate the coefficients and $\mathcal{O}(N^3)$ operations to solve Eq. (11) if a direct solver is employed. In addition, the size of required memory for storing $\bar{\mathbf{A}}$ is also proportional to $\mathcal{O}(N^2)$. For multi-frequency acoustic analyses, Eq. (11) needs to be repeatedly formed and solved across the frequency range of interest, which limits the application of traditional BEM in solving large-scale acoustic problems. This fact motivates the use of model order reduction techniques, which aims at reducing the system dimensions (and the associated computational effort and storage) while still capturing key dynamical behavior and preserving essential properties of the original large-scale model.

3.1. Frequency decoupling

However, the difficulty in applying MOR schemes to acoustic BE systems is that their coefficient matrix has a frequency-dependent property. For the purpose of model reduction the system matrices and projection operators are expected to be irrespective of the frequency. Therefore, one must take out of the wavenumber from the exponential function in the fundamental solution (and its normal and partial derivatives) such that frequency-independent integrands in Eqs. (4) and (7) can be realized. Luckily, as this dependence is typically affine, it is possible to use Taylor's theorem about a fixed expansion point $k_\circ$ to fulfill this decomposition

$$\mathrm{e}^{\mathrm{j}kr} = \mathrm{e}^{\mathrm{j}k_\circ r} \sum_{m=0}^{\infty} \frac{(\mathrm{j}r)^m (k-k_\circ)^m}{m!}. \tag{13}$$

In order to comply with the actual physical meaning, the choice of a purely real number for $k_\circ$ is suggested. In practice, the infinite order series should be truncated to a finite order, which introduces the approximation error. If we apply Taylor expansion with $M+1$ terms (i.e. from order 0 to order M), the error bound based on the Lagrange remainder over a boundary element $\Delta\Gamma$ can be practically defined as:

$$\delta = \int_{\Delta\Gamma} \frac{[\mathrm{j}r(k-k_\circ)]^{M+1}}{(M+1)!} \mathrm{e}^{\mathrm{j}\hat{k}r}\, \mathrm{d}\Gamma \le \left| \frac{[r_\mathrm{d}(k-k_\circ)]^{M+1}}{(M+1)!} S_{\max} \right| < \varepsilon \tag{14}$$

in which $\hat{k} \in (k_\circ, k)$; r_d is the largest distance between the field point and source point, which is determined by the topological shape of underlying structure; $S_{\max}$ is the maximum area of surface element; ε is the user-specified tolerance. This empirical error bound can be used in advance to estimate the suitable number of expansion terms required for a desired level of accuracy.

If the considered frequency range is too wide or the size of structures is too large, which leads to many terms of Taylor series to accurately represent the kernels. In these cases, the entire broadband frequency range of interest can be divided into several frequency subintervals. Within each interval, a single-point expansion around its middle frequency is applied and then the following MOR technique can be used to accelerate the numerical simulation without any limitation, as detailed in the proceeding section.

3.2. Reformulation

Depending on the boundary conditions, the CBIE in Eq. (4) and HBIE in Eq. (7) along with Eq. (10) are reorganized for the sake of clarity.

3.2.1. Neumann boundary condition

Substituting Eq. (13) into Eq. (10) and according to the order of k, the system of equations can be reformulated in an equivalent form as

$$\left[\sum_{m=0}^{M} \frac{(k-k_\star)^m}{m!} (k^2\mathbf{M}_m + k\mathbf{D}_m + \mathbf{K}_m) \right] \mathbf{p} = \mathbf{b}_\mathrm{v}, \tag{15}$$

where

$$\begin{aligned}\mathbf{M}_m &= \int_\Gamma (\mathrm{j}r)^m \left[\beta \frac{\mathrm{e}^{\mathrm{j}k_\star r}}{4\pi r}\frac{\partial r}{\partial n(\mathbf{x})}\frac{\partial r}{\partial n(\mathbf{y})}\right] \mathrm{d}\Gamma, \qquad \mathbf{D}_m = -\mathrm{j}r\mathbf{K}_m = -\mathbf{K}_{m+1},\\ \mathbf{K}_m &= \int_\Gamma (\mathrm{j}r)^m \left[\beta \frac{\mathrm{e}^{\mathrm{j}k_\star r}}{4\pi r^3}(n_i(\mathbf{x})n_i(\mathbf{y}) - 3\frac{\partial r}{\partial n(\mathbf{x})}\frac{\partial r}{\partial n(\mathbf{y})}) - \frac{\mathrm{e}^{\mathrm{j}k_\star r}}{4\pi r^2}\frac{\partial r}{\partial n(\mathbf{y})}\right] \mathrm{d}\Gamma.\end{aligned} \tag{16}$$

Note the difference between $k_\circ$ and $k_\star$, where $k_\circ$ is a single expansion point used to approximate the kernels over the considered frequency range, while $k_\star$ represent three expansion points used to construct a global orthonormal basis, as given below. In addition, in Eq. (15), $(k-k_\star)^m/m!$ instead of $(k-k_\star)^m$ are extracted from integrands such that the values in the frequency-decoupled system matrices are roughly consistent without rounding error. These expressions can be readily obtained by means of the $H(\mathbf{x},\mathbf{y})$ and $F(\mathbf{x},\mathbf{y})$ kernels. Furthermore, the relationship between $\mathbf{K}_{m+1}$ and $\mathbf{D}_m$ can be used to save the computational time and memory consumption. The right hand side $\mathbf{b}_\mathrm{v}$ of Eq. (15) can be similarly obtained. For example, a special case is the acoustically rigid BC, where the prescribed value for normal velocity $\bar{v}_n$ is zero. In this case, we have $\mathbf{b}_\mathrm{v} = \mathbf{b}^\mathrm{I}$.

With the frequency decoupling technique, the frequency-dependent system matrices in Eq. (10) are now decomposed into the sum of frequency-dependent scalar functions multiplied by frequency-independent system matrices $\mathbf{M}_m$, $\mathbf{D}_m$ and $\mathbf{K}_m$. In obvious, the integral calculations of them need to be carried out only once and the subsequent frequency sweep process can thus be expedited. However, this technique quickly becomes intractable as the size of involved model grows. This is because these dense frequency-independent system matrices have to be stored and then used simultaneously in the online matrix assembly of the whole BE system for each frequency, where the required storage scales with $\mathcal{O}((2M+3)N^2)$.

A remedy to cope with the arising memory problem is to use MOR techniques in such a way that a low-dimensional subspace (spanned by an orthonormal basis) is constructed to define a reduced-order model. The resulting surrogate model with a much smaller size should contain sufficient information about the essential dynamics of original BE system and meanwhile hold the same form as formulated in Eq. (15). Different approaches differ in how the orthonormal basis is constructed. Since the Helmholtz equation is a second-order linear partial differential equation, in this work, the moment-matching method based on the efficient second-order Arnoldi procedure [31] is applied. To this end, only the system matrices corresponding to the selected expansion point $k_\star$ in the series expanded Eq. (15) is used to implement the SOAR algorithm to iteratively generate a frequency-independent orthonormal basis. To be more specific, we have the following

$$[k^2\mathbf{M}_\mathrm{v} + k\mathbf{D}_\mathrm{v} + \mathbf{K}_\mathrm{v}]\mathbf{p} = \mathbf{b}_\mathrm{v}. \tag{17}$$

The integration expressions of matrices $\mathbf{M}_\mathrm{v}$, $\mathbf{D}_\mathrm{v}$ and $\mathbf{K}_\mathrm{v}$ can be easily obtained from Eq. (16) by setting $m=0$, i.e. $\mathbf{M}_\mathrm{v} = \mathbf{M}_0$, $\mathbf{D}_\mathrm{v} = \mathbf{D}_0$ and $\mathbf{K}_\mathrm{v} = \mathbf{K}_0$. One would wonder why the system matrices around the expansion point can be used to construct an orthonormal basis with sufficient accuracy for projection. The reason is because entries in different $\mathbf{M}_m$ or $\mathbf{D}_m$ or $\mathbf{K}_m$ differ by only one coefficient $\mathrm{j}r$. Therefore, the system matrices $\mathbf{M}_\mathrm{v}$, $\mathbf{D}_\mathrm{v}$ and $\mathbf{K}_\mathrm{v}$ without more derivative matrices in fact maintain inherent information about the original system of equations. Before the SOAR algorithm is presented in detail to improve the computational efficiency, we show how to obtain another system with the same second-order structure as in Eq. (17) for a 3D Helmholtz problem under pressure boundary condition.

3.2.2. Dirichlet boundary condition

Analogously, making use of Eq. (13) and rearranging the $G(\mathbf{x},\mathbf{y})$ and $E(\mathbf{x},\mathbf{y})$ kernels with respect to the order of wavenumber k yield

$$\left[\sum_{m=0}^{M}\frac{(k-k_\star)^m}{m!}(k\mathbf{V}_m + \mathbf{W}_m)\right]\mathbf{q} = \mathbf{b}_\mathrm{p}, \tag{18}$$

where

$$\begin{aligned}\mathbf{V}_m &= \int_\Gamma (\mathrm{j}r)^m \left[-\mathrm{j}\beta \frac{\mathrm{e}^{\mathrm{j}k_\star r}}{4\pi r}\frac{\partial r}{\partial n(\mathbf{x})}\right] \mathrm{d}\Gamma,\\ \mathbf{W}_m &= \int_\Gamma (\mathrm{j}r)^m \left[\frac{\mathrm{e}^{\mathrm{j}k_\star r}}{4\pi r^2}(r + \beta\frac{\partial r}{\partial n(\mathbf{x})})\right] \mathrm{d}\Gamma.\end{aligned} \tag{19}$$

In a similar fashion, the right hand side $\mathbf{b}_\mathrm{p}$ of Eq. (18) can also be obtained. A special case is the sound soft BC with zero value for prescribed pressure $\bar{p}$ on a subject surface. In this case, one has $\mathbf{b}_\mathrm{p} = -\mathbf{b}^\mathrm{I}$. For this problem, the memory required by the series expansion is $\mathcal{O}(2(M+1)N^2)$.

Eq. (18) is obviously different from the one for velocity BC as given in Eq. (15). When $m = 0$, a linear dynamical system is of the form

$$[k\mathbf{V}_0 + \mathbf{W}_0]\,\mathbf{q} = \mathbf{b}_\mathrm{p}. \tag{20}$$

Then the standard (linear) Krylov subspace-based methods for moment-matching reduced order modeling of large-scale linear systems can be applied, where the orthonormal basis can be constructed via the Arnoldi or Lanczos iteration process [24–26]. In this work, instead of using the linear system, we construct a second-order system as in Eq. (17) to unify the model reduction process for BE systems with different BCs. That is to say, the well-developed SOAR algorithm can also be directly exploited for computational efficiency. To do this, the two kernels $G(\mathbf{x},\mathbf{y})$ and $E(\mathbf{x},\mathbf{y})$ around a fixed expansion point $k_\star$ is approximated by linearization

$$\begin{aligned} G(\mathbf{x},\mathbf{y}) =& \frac{\mathrm{e}^{\mathrm{j}kr}}{4\pi r} \approx \frac{\mathrm{e}^{\mathrm{j}k_\star r}}{4\pi r}(1 - \mathrm{j}k_\star r + \mathrm{j}kr), \\ E(\mathbf{x},\mathbf{y}) =& \frac{\mathrm{e}^{\mathrm{j}kr}}{4\pi r^2}(1-\mathrm{j}kr)\frac{\partial r}{\partial n(\mathbf{x})} \approx \frac{\mathrm{e}^{\mathrm{j}k_\star r}}{4\pi r^2}(1 - \mathrm{j}k_\star r - k_\star k r^2 + k^2 r^2)\frac{\partial r}{\partial n(\mathbf{x})}. \end{aligned} \tag{21}$$

Then the system of equations subjected to the Dirichlet BC can be easily derived as

$$\left[k^2\mathbf{M}_\mathrm{p} + k\mathbf{D}_\mathrm{p} + \mathbf{K}_\mathrm{p}\right]\mathbf{q} = \mathbf{b}_\mathrm{p}, \tag{22}$$

where

$$\begin{aligned} \mathbf{M}_\mathrm{p} &= \int_\Gamma \left[\frac{\mathrm{e}^{\mathrm{j}k_\star r}}{4\pi}\beta\frac{\partial r}{\partial n(\mathbf{x})}\right]\mathrm{d}\Gamma, \quad \mathbf{D}_\mathrm{p} = \int_\Gamma \left[\frac{\mathrm{e}^{\mathrm{j}k_\star r}}{4\pi}(\mathrm{j} - \beta k_\star\frac{\partial r}{\partial n(\mathbf{x})})\right]\mathrm{d}\Gamma, \\ \mathbf{K}_\mathrm{p} &= \int_\Gamma \left[\frac{\mathrm{e}^{\mathrm{j}k_\star r}}{4\pi r^2}(1-\mathrm{j}k_\star r)(r + \beta\frac{\partial r}{\partial n(\mathbf{x})})\right]\mathrm{d}\Gamma. \end{aligned} \tag{23}$$

or equivalently, one can also represent the system matrices as

$$\mathbf{M}_\mathrm{p} = \mathbf{V}_1, \quad \mathbf{D}_\mathrm{p} = \mathbf{V}_0 - k_\star\mathbf{V}_1 + \mathbf{W}_1, \quad \mathbf{K}_\mathrm{p} = \mathbf{W}_0 - k_\star\mathbf{W}_1. \tag{24}$$

Since the second-order system of equations for the construction of reduction basis have been prepared, the basic concept of the SOAR algorithm and its straightforward implementation will be introduced in the following.

3.3. SOAR procedure

Eqs. (17) and (22) can be expressed in a unified way as

$$\left[k^2\mathbf{M}_* + k\mathbf{D}_* + \mathbf{K}_*\right]\mathbf{z} = \mathbf{b}_*, \tag{25}$$

with the subscript $* = \mathrm{v}$ for the Neumann boundary case and $* = \mathrm{p}$ for the Dirichlet boundary case. $\mathbf{z}$ ($= \mathbf{p}$ or $\mathbf{q}$) indicates the unknown node vector as defined in Eq. (11). It should be underlined that Eq. (25) is only used to construct a frequency-independent orthonormal basis such that both Eqs. (15) and (18) can be projected onto the spanned subspace.

By replacing k with the wavenumber-shifted variable $k - k_\star$, Eq. (25) can be rewritten as

$$\left[(k-k_\star)^2\tilde{\mathbf{M}} + (k-k_\star)\tilde{\mathbf{D}} + \tilde{\mathbf{K}}\right]\mathbf{z} = \mathbf{b}_*. \tag{26}$$

Comparing the coefficients between Eqs. (25) and (26) results in

$$\tilde{\mathbf{M}} = \mathbf{M}_*, \quad \tilde{\mathbf{D}} = 2k_\star\mathbf{M}_* + \mathbf{D}_*, \quad \tilde{\mathbf{K}} = k_\star^2\mathbf{M}_* + k_\star\mathbf{D}_* + \mathbf{K}_*. \tag{27}$$

It has been found that the second-order Arnoldi algorithm offers an elegant way to generate a desired reduction basis $\mathbf{Q}_\star$ with $\mathbf{r}_0 \neq 0$ for large-scale second-order dynamical systems:

$$\mathrm{span}\{\mathbf{Q}_\star\} = \mathcal{G}_{n_\star}(\mathbf{A},\mathbf{B};\mathbf{r}_0) = \mathrm{span}\{\mathbf{r}_0,\mathbf{r}_1,\mathbf{r}_2,\ldots,\mathbf{r}_{n_\star-1}\} \tag{28}$$

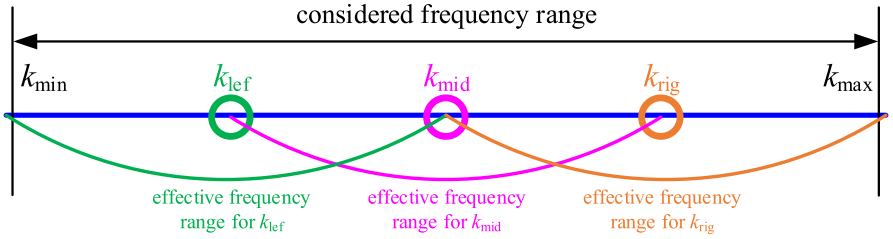

Fig. 1. The three selected expansion points and their desired convergence radius.

where

$$\begin{cases} \mathbf{r}_1 = \mathbf{A}\mathbf{r}_0, \\ \mathbf{r}_\iota = \mathbf{A}\mathbf{r}_{\iota-1} + \mathbf{B}\mathbf{r}_{\iota-2}, \quad \text{for } \iota \geq 2 \end{cases} \tag{29}$$

and the sequence $\mathbf{r}_0, \mathbf{r}_1, \mathbf{r}_2, \ldots, \mathbf{r}_{n_\star-1}$ is called a second-order Krylov sequence based on a pair of matrices $\mathbf{A} = -\tilde{\mathbf{K}}^{-1}\tilde{\mathbf{D}}$ and $\mathbf{B} = -\tilde{\mathbf{K}}^{-1}\tilde{\mathbf{M}}$ and a starting vector $\mathbf{r}_0 = \tilde{\mathbf{K}}^{-1}\mathbf{b}_*$, where the modified Gram–Schmidt process is used to orthogonalize them and check the linear dependence. Such a subspace $\mathcal{G}_{n_\star}(\mathbf{A}, \mathbf{B}; \mathbf{r}_0)$ is called an $n_\star$th second-order Krylov subspace since the vector $\mathbf{r}_\iota$ is obtained by a linear homogeneous recurrence relation of degree 2 [31]. $\mathbf{Q}_\star \in \mathbb{C}^{N\times n_\star}$ denotes the orthonormal and frequency-independent basis matrix, which is composed of $n_\star$ number of nonzero column vectors. In most cases, it holds that $n_\star \ll N$. The processing time for calculating the inverse of matrix $\tilde{\mathbf{K}}$ and subsequent matrix–vector multiplications can be accelerated using an LU factorization.

4. Adaptive procedure, projection and online solution

Before we proceed to the use of the second-order Krylov subspace as the projection subspace to define a dimension reduced system, we discuss how to construct a reliable global orthonormal basis in an automatic way.

4.1. Determination of the expansion point and its associated order

For frequency sweep analysis of BE problems, one hopes that the response of the constructed ROM is sufficiently close to that of the original FOM. Under this condition, the following should be satisfied.

$$\frac{|y - \hat{y}_n|}{|y|} \leq \frac{|y - \hat{y}|}{|y|} + \frac{|\hat{y} - \hat{y}_n|}{|y|} < \varepsilon \tag{30}$$

in which y and $\hat{y}$ describe the input–output behavior of the original BE system without and with the Taylor series expansion of the Green's function, respectively; $\hat{y}_n$ is the transfer function obtained from the ROM.

As described in Eq. (30), there are two main contributions in the overall approximation error. One is the truncation error in decoupling the frequency, which can be evaluated by Eq. (14). The second error is the reduction error in the classical sense, which originates from projecting the frequency-decoupled FOM onto a low-dimensional subspace. In general, a knowledge of the second exact relative error is difficult to achieve *a priori*. Recall from the Introduction that an error indicator based on the input/output residual or difference between two ROMs is not appropriate for dense BE system matrices.

In the SOAR procedure, increasing the number of basis vectors for a fixed expansion point is much less expensive than starting a new expansion point which suffers from the necessity of the inverse of matrix $\tilde{\mathbf{K}}$. Therefore, a very limited number of expansion points is expected to economize the offline construction of an orthonormal basis. In addition, a single-point expansion is often not enough to capture dynamical characteristics of the FOM in the frequency range away from the chosen point due to the local approximation property of Taylor's theorem. Therefore, in this work, three expansion points are discretely deployed around $k_{\text{lef}} = (3k_{\min} + k_{\max})/4$, $k_{\text{mid}} = (k_{\min} + k_{\max})/2$ and $k_{\text{rig}} = (k_{\min} + 3k_{\max})/4$, where $k_{\min} = 2\pi f_{\min}/c$ and $k_{\max} = 2\pi f_{\max}/c$ are the wavenumbers associated with the frequencies located at the left and right endpoints of the considered frequency band, as shown in Fig. 1. The above-mentioned subscript $\star$ (= lef/mid/rig) indicates that variables are related to the left, middle and right expansion points from here onward. Then, according to Eq. (14), the truncated order of Taylor series expansion $\hat{M}$

for separately valid frequency interval (i.e. $[k_{\min}, k_{\mathrm{mid}}]$, $[k_{\mathrm{lef}}, k_{\mathrm{rig}}]$, $[k_{\mathrm{mid}}, k_{\max}]$ or slightly wider) can be decided. It is noted that $\hat{M}$ is the same owing to the uniform frequency spacing. This provides a fair opportunity for each of the expansion points to converge within their own radius of accuracy. After that, the success of an adaptive scheme just depends on the number of orthonormal basis vectors to be calculated for each $k_\star$.

The next important step is to specify the order of orthonormal basis corresponding to k_{lef}, k_{mid} and k_{rig}. The scalar transfer function y of Eq. (12) is a rational function. An intuitive way to generate a representation of y is to use Taylor's theorem [25], which leads to a power series form as

$$y = \mathbf{L}^{\mathrm{T}}\bar{\mathbf{A}}^{-1}\mathbf{b} = \sum_{\ell=0}^{\infty}(k-k_\star)^{\ell} y_\ell, \tag{31}$$

where y_ℓ for $\ell \geq 0$ are called moments about $k_\star$. It should be mentioned here that since the computation cost of $\mathbf{L}$ is relatively low, we use a direct solution as in the conventional BEM to obtain it for calculation accuracy. Note that $\bar{\mathbf{A}}$ is approximated by the series expansion and truncated as

$$\bar{\mathbf{A}} = \sum_{m=0}^{\hat{M}}(k-k_\star)^{m}\bar{\mathbf{A}}_m, \tag{32}$$

where $\bar{\mathbf{A}}_m$ is a set of frequency-independent polynomial matrix [44]. Substituting Eq. (32) into Eq. (11) and multiplying Eq. (11) with $\mathbf{A}_0^{-1}$ from the left side, the transfer function of the frequency-decoupled system can be cast into the form

$$\hat{y} = \mathbf{L}^{\mathrm{T}}[\mathbf{I} - \sum_{m=1}^{\hat{M}}(k-k_\star)^{m}(-\bar{\mathbf{A}}_0^{-1}\bar{\mathbf{A}}_m)]^{-1}\bar{\mathbf{A}}_0^{-1}\mathbf{b} = \sum_{\ell=0}^{\infty}(k-k_\star)^{\ell}\hat{y}_\ell. \tag{33}$$

The error between y and $\hat{y}$ can be estimated as mentioned before, i.e. $y-\hat{y} = \mathcal{O}((k-k_\star)^{\hat{M}})$ with Peano form of the remainder. Accordingly, the ℓ for $\hat{y}$ in Eq. (33) can be truncated to $\hat{M}$, i.e. to match the first $\hat{M}+1$ moments of y. The objectives of a moment-matching MOR method are to construct a reduced system whose moments match the moments of the original large-scale system as much as possible and meanwhile to preserve (to the possible extent) its important properties and physical meaning. Since we only use the (second-order) system matrices around the selected expansion point to construct an orthonormal basis, the expansion of its transfer function as in Eq. (33) will result in a maximum order of $2\hat{M}$ (which can be roughly regarded as an extension of $1/(1-x) = 1+x+x^2+\cdots$ from number to matrix). According to Ref. [45], if the SOAR procedure manually stops at the $(2\hat{M})$th step, then the transfer function $\hat{y}_n$ of the reduced model is an $(2\hat{M}+1)$th Padé-type approximant of the transfer function of the nonsymmetric second-order system in Eq. (25). Therefore, in what follows, we set the supremum of order for each expansion point to $2\hat{M}$. In fact, this setting is not so important because it will be truncated (prematurely) by the following (condition number) criterion.

It has been noticed that the SOAR algorithm will stagnate in accuracy when a certain value of order is reached. In this case, it is impractical to approximate the FOM better by using more orthonormal projection vectors in the slow convergence range. This is due to the fact that the condition number of the triangular matrix in the SOAR algorithm usually grows quickly, which leads to numerical instability [46]. This phenomenon together with the pre-specified termination tolerance ε can be utilized to automatically select the dimension of the reduced system.

Algorithm 1 describes the pseudocode of the proposed AT-SOAR procedure. Through application of the SOAR algorithm with j steps, $j+1$ columns of orthonormal vectors spanning the second-order Krylov subspace $\mathcal{G}_{j+1}(\mathbf{A}, \mathbf{B}; \mathbf{r}_0)$ are generated. Note that at line 4 of the algorithm, the supremum of order for each expansion point is $2\hat{M}$, as explained above. At line 20, lub/ε denotes the set upper bound on the condition number of the upper Hessenberg matrix $\hat{\mathbf{T}}$, which is also relevant to the accuracy threshold ε. Unless otherwise stated, the default value lub = 1e3 is used as the stopping criterion for each expansion point $k_\star$. This adaptive strategy is favored for large-scale problems because of its quite simple and straightforward implementation without resort to the FOM and comparison of different ROMs.

As the three expansion points have their own local reduction basis, an orthogonalization procedure should be applied to combine them into a union of reduction bases generated from multiple second-order Krylov subspaces.

Algorithm 1 Adaptive SOAR procedure

Input: $\mathbf{A}$, $\mathbf{B}$, $\mathbf{r}_0$; **Output:** $\mathbf{Q}_\star$ for selected $k_\star$ with $\star$ being [lef, mid, rig]

preallocate $\mathbf{Q} = \text{zeros}(N, 2\hat{M}+1)$, $\hat{\mathbf{T}} = \text{zeros}(2\hat{M}+1, 2\hat{M}+1)$
$\mathbf{q}_1 = \mathbf{r}_0/\|\mathbf{r}_0\|_2$
$\mathbf{f} = \mathbf{0}$
for $j = 1, 2, \cdots, 2\hat{M}$ **do**
  $\mathbf{r} = \mathbf{A}\mathbf{q}_j + \mathbf{B}\mathbf{f}$
  for $i = 1, 2, \cdots, j$ **do**
    $t_{ij} = \mathbf{q}_i^{\mathrm{H}}\mathbf{r}$
    $\mathbf{r} = \mathbf{r} - \mathbf{q}_i t_{ij}$
  end for
  $t_{j+1,j} = \|\mathbf{r}\|_2$
  if $t_{j+1,j} \neq 0$ **then**
    $\mathbf{q}_{j+1} = \mathbf{r}/t_{j+1,j}$
    $\mathbf{f} = \mathbf{Q}_j\hat{\mathbf{T}}(2:j+1, 1:j)^{-1}\mathbf{e}_j$
  else
    reset $t_{j+1,j} = 1$
    $\mathbf{q}_{j+1} = \mathbf{0}$
    $\mathbf{f} = \mathbf{Q}_j\hat{\mathbf{T}}(2:j+1, 1:j)^{-1}\mathbf{e}_j$
    save $\mathbf{f}$ and check breakdown
  end if
  if $\text{cond}(\hat{\mathbf{T}}(1:j, 1:j), 1) > \text{lub}/\varepsilon$ **then**
    break
  end if
end for
$\mathbf{Q}_\star = \mathbf{Q}_{j+1}$

Notations: $\|\bullet\|_2$ represents 2-norm of a vector or matrix, cond($\bullet$, 1) returns the 1-norm condition number of a matrix, $\mathbf{e}_j$ is the jth column of the identity matrix $\mathbf{I}$, $\mathbf{0}$ denotes a zero vector or matrix, $\hat{\mathbf{T}}$ is an upper Hessenberg matrix.

In this way, a global orthonormal basis matrix with multi-point moment-matching properties can be achieved as

$$\mathbf{Q} = \text{orth}([\mathbf{Q}_{\text{lef}}, \mathbf{Q}_{\text{mid}}, \mathbf{Q}_{\text{rig}}]), \qquad \mathcal{G}_{n_{\text{lef}}} \cup \mathcal{G}_{n_{\text{mid}}} \cup \mathcal{G}_{n_{\text{rig}}} = \text{span}\{\mathbf{Q}\}. \tag{34}$$

So far, the global orthonormal basis $\mathbf{Q} \in \mathbb{C}^{N\times n}$ used for projection has been established, where n is the order of the final reduced model (or DOFs of the ROM). Next, dynamical systems described by Eqs. (15) and (18) are to be projected onto the spanned low-dimensional subspace over the whole frequency range of interest.

4.2. Column by column projection

First, the system matrices around the middle expansion point $k_\circ = k_{\text{mid}}$ has already been formed for the purpose of constructing a reduction basis, thus part of the ROM with $m = 0$ for the Neumann BC or with $m = 0$ and 1 for the Dirichlet BC can be readily built via projection. Then a complete ROM can be obtained by using a congruence transformation on those remaining frequency-independent series representations.

However, this is not really a memory-efficient solution process as the dense system matrices need to be explicitly formed. Storing these matrices requires $\mathcal{O}((2M+1)N^2)$ entries for the Neumann BC and $\mathcal{O}(2(M-1)N^2)$ for the Dirichlet BC, which may quickly exceed the available memory. Note that the relation between $\mathbf{K}_{m+1}$ and $\mathbf{D}_m$ in Eq. (16) is used such that the storage of $\mathcal{O}((2M+1)N^2)$ rather than $\mathcal{O}(3MN^2)$ is given. Therefore, a memory saving column-by-column projection is applied. In other words, once one column in the BE frequency-decoupled matrices is assembled for one field point and all the source points, a left-sided projection is immediately implemented until all the field points are computed. In this way, the required storage for the Neumann BC is reduced from

$\mathcal{O}((2M+1)N^2)$ to $\mathcal{O}((2M+1)nN)$, followed by a right-sided projection for the resulting matrices, the memory usage is further reduced to $\mathcal{O}((2M+1)n^2)$. With regard to the Dirichlet BC, the memory requirement is also decreased from $\mathcal{O}(2(M-1)N^2)$ to $\mathcal{O}(2(M-1)nN)$ and further to $\mathcal{O}(2(M-1)n^2)$ via the MOR technique. As a by-product, the projection step via the congruence transformations can potentially yield better conditioned systems as multiplying with an orthonormal matrix on both sides of the system matrices can be viewed as preconditioning.

It should be admitted here that as any typical acoustic scattering problem, the right-hand side of system of equations depends on the wavenumber. To this effect, the forcing vector, e.g. a plane incident wave $\mathbf{b}^{\mathrm{I}}$, has to be projected in the frequency sweep stage, which undermines the online computational efficiency. However, this impact is small and can thus be negligible.

Algorithm 2 Offline projection for the Neumann BC

1: $\mathbf{M}_{0nn} = \mathbf{Q}^{\mathrm{H}}\mathbf{M}_{\mathrm{v}}\mathbf{Q}$, $\mathbf{D}_{0nn} = \mathbf{Q}^{\mathrm{H}}\mathbf{D}_{\mathrm{v}}\mathbf{Q}$, $\mathbf{K}_{0nn} = \mathbf{Q}^{\mathrm{H}}\mathbf{K}_{\mathrm{v}}\mathbf{Q}$
2: **for** $j = 1, 2, \cdots, N$ **do**
3: **for** $i = 1, 2, \cdots, N$ **do**
4: **if** $i \neq j$ **then**
5: numerical Gaussian quadrature of the kernels
6: **else**
7: analytical integration of the kernels
8: **end if**
9: **end for**
10: **for** $m = 1, 2, \cdots, M$ **do**
11: $\mathbf{m}_{mnj} = \mathbf{Q}^{\mathrm{H}}\mathbf{m}_{mN}$, $\mathbf{k}_{mnj} = \mathbf{Q}^{\mathrm{H}}\mathbf{k}_{mN}$
12: **end for**
13: $\mathbf{k}_{(M+1)nj} = \mathbf{Q}^{\mathrm{H}}\mathbf{k}_{(M+1)N}$
14: **end for**
15: **for** $m = 1, 2, \cdots, M$ **do**
16: $\mathbf{M}_{mnn} = \mathbf{M}_{mnN}\mathbf{Q}$, $\mathbf{K}_{mnn} = \mathbf{K}_{mnN}\mathbf{Q}$
17: **end for**
18: $\mathbf{K}_{(M+1)nn} = \mathbf{K}_{(M+1)nN}\mathbf{Q}$

Notations: $\bullet^{\mathrm{H}}$ designates the Hermitian transpose, lower case letters such as $\mathbf{m}$ denote a column of vector and capital letters such as $\mathbf{M}$ denote a matrix. In the **if**-loop (lines 4-8), different e.g. $\mathbf{m}_m$ differ by only the coefficient jr, thus vectorization operation can be used to avoid **for**-loop.

Since forming the system matrices explicitly is no longer necessary, a fast and low-memory projection for the implementation of the proposed AT-SOAR technique can be accomplished. A summary of the projection procedure for different BCs is respectively presented in Algorithms 2 and 3, where the diagonal ingredients of the system matrices are obtained by using the analytical integration [47]. It should be emphasized that the transformed matrix triplet ($\tilde{\mathbf{M}}$, $\tilde{\mathbf{D}}$, $\tilde{\mathbf{K}}$) in Eq. (27) is used to generate the global frequency-independent orthonormal basis $\mathbf{Q}$ of the projection subspace $\mathcal{G}_n$, but the original matrices and vectors in Eqs. (15) and (18) are directly projected onto the same subspace $\mathcal{G}_n$ without loss of generality.

4.3. Online multi-frequency analysis

In the online frequency sweep phase, we need to compute the frequency-dependent coefficients in Eqs. (15) and (18) for each frequency and then a robust ROM can be rapidly created from the offline stored reduced matrices/vectors. Then a built-in solver in Matlab (i.e. `backslash`) is used to solve the reduced system of equations. In this way, the required CPU time is predictable and it only relies on the dimension of the ROM, thereby reducing the computational complexity dramatically compared to the brute direct solution of the high-dimensional original model. In addition, through application of the structure-preserving dimension reduction technique, the form of frequency-decoupled system of equations in Eqs. (15) and (18) is preserved.

In conclusion, the proposed AT-SOAR approach falls into the offline–online reduced-order modeling framework. In the offline phase, the second-order Krylov subspace as the projection subspace with a much smaller dimension

Algorithm 3 Offline projection for the Dirichlet BC

1: $\mathbf{M}_{0nn} = \mathbf{Q}^{\mathrm{H}}\mathbf{M}_{\mathrm{p}}\mathbf{Q}$, $\mathbf{D}_{0nn} = \mathbf{Q}^{\mathrm{H}}\mathbf{D}_{\mathrm{p}}\mathbf{Q}$, $\mathbf{K}_{0nn} = \mathbf{Q}^{\mathrm{H}}\mathbf{K}_{\mathrm{p}}\mathbf{Q}$
2: **for** $j = 1, 2, \cdots, N$ **do**
3: **for** $i = 1, 2, \cdots, N$ **do**
4: **if** $i \neq j$ **then**
5: numerical Gaussian quadrature of the kernels
6: **else**
7: analytical integration of the kernels
8: **end if**
9: **end for**
10: **for** $m = 2, 3, \cdots, M$ **do**
11: $\mathbf{v}_{mnj} = \mathbf{Q}^{\mathrm{H}}\mathbf{v}_{mN}$, $\mathbf{w}_{mnj} = \mathbf{Q}^{\mathrm{H}}\mathbf{w}_{mN}$
12: **end for**
13: **end for**
14: **for** $m = 2, 3, \cdots, M$ **do**
15: $\mathbf{V}_{mnn} = \mathbf{V}_{mnN}\mathbf{Q}$, $\mathbf{W}_{mnn} = \mathbf{W}_{mnN}\mathbf{Q}$
16: **end for**

Notations: with Eq. (24), the entire reduced frequency-decoupled system matrices can be obtained via the combination of line 1 and line 15.

than the full-order problem, is spanned by a set of orthonormal vectors, which is recursively obtained via the SOAR algorithm. As a support, an adaptive scheme is incorporated into the framework to advance the present technique. Once the reduction basis is constructed, a column-by-column projection is further sought to favor the overall memory requirements. In the online phase, fast frequency sweep analysis with significant acceleration can be achieved because it does not involve any costly dense matrix operation.

5. Numerical results and discussion

In this section, we present three numerical cases to demonstrate the high performance of the AT-SOAR solution procedure for solving large-scale acoustic BE systems. All our codes are implemented in Matlab R2019a. All numerical tests are performed on a Windows Machine with Intel(R) Xeon(R) Gold 6132 CPU at 2.60 GHz and 64 GB of RAM.

For the first two academic examples, the medium of acoustic field is assumed to be air whose mass density and speed of sound are respectively taken as $\rho = 1.29$ kg/m^3 and $c = 343$ m/s. As the last more complicated application, the scatterer is surrounded by an infinite domain of water with a density of 1000 kg/m^3 and speed of sound of 1500 m/s.

5.1. Scattering from a rigid sphere

The first example is a classical benchmark model, which comprises a rigid sphere with radius $R = 1$ m submerged in air, as shown in Fig. 2. This sphere is impinged upon by a plane incident wave with unit amplitude along the global positive x-direction, i.e. $p^{\mathrm{I}}(\mathbf{x}) = \mathrm{e}^{\mathrm{j}kx}$. The analytical solution for the total sound pressure is available [48], which is the sum of the incident (p^{I}) and scattered (p^{S}) acoustic waves with a series of spherical harmonics

$$p(r,\theta) = \sum_{l=0}^{\infty} \mathrm{j}^l (2l+1) j_l(kr) P_l(\cos\theta) - \sum_{l=0}^{\infty} \mathrm{j}^l (2l+1) \frac{j_l'(kR)}{h_l'(kR)} h_l(kr) P_l(\cos\theta), \tag{35}$$

where j_l' and h_l' are the derivatives of spherical Bessel function j_l and Hankel function h_l, respectively; P_l is the Legendre polynomial of order l; r is the distance from the sphere center; the angle θ is defined such that the shadow zone is located at $\theta = 0$.

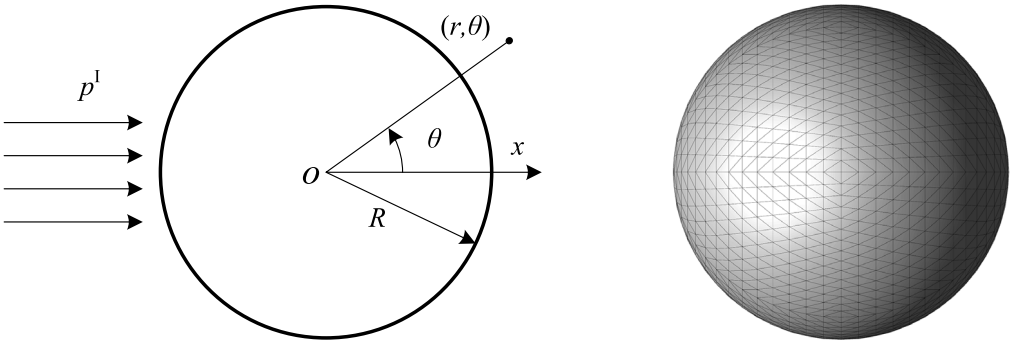

Fig. 2. (a) Plane wave scattered by a sphere and (b) its BE mesh.

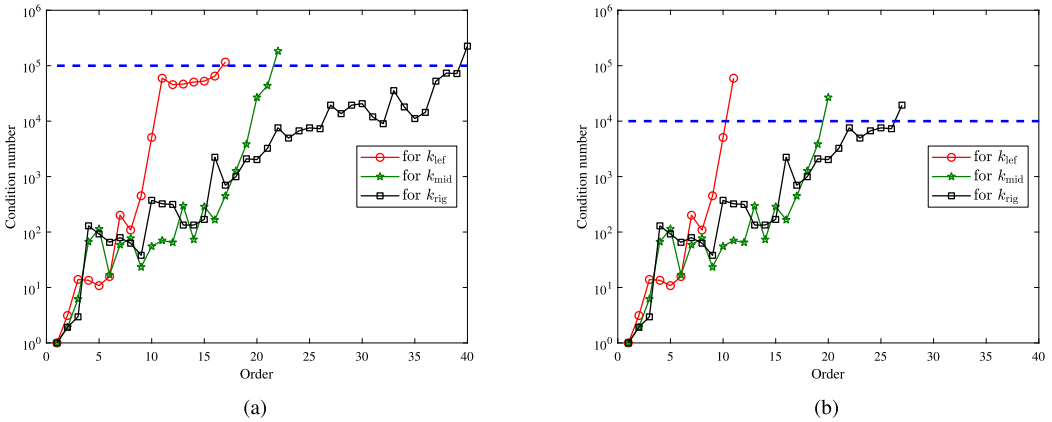

Fig. 3. Condition number of $\hat{\mathbf{T}}$ with respect to the number of order: (a) case 1 with $\varepsilon = 0.01$; (b) case 2 with $\varepsilon = 0.1$.

The surface of sphere is meshed with 2700 constant triangular elements, which results in a BE dynamical system of order $N = 2700$. The exterior-field total sound pressure responses $|p(r,\theta)|$ for the following two cases are simulated from $f_{\min} = 1$ Hz to $f_{\max} = 1000$ Hz with frequency step of 1 Hz:

case 1: at the point $(r = 2R, \theta = \pi/2)$ with prescribed threshold $\varepsilon = 0.01$;

case 2: at the point $(r = 5R, \theta = \pi)$ with prescribed threshold $\varepsilon = 0.1$.

In this example, the largest distance r_{d} as defined in Eq. (14) is the diameter of sphere, i.e. $r_{\mathrm{d}} = 2$ m. According to the derived error bound, the maximum expansion terms $M = 46$ for case 1 and $M = 43$ for case 2 around the selected $k_{\circ}$ $(= k_{\mathrm{mid}})$ are sufficient for obtaining reliable solution within the considered frequency range.

In order to construct a proper projection subspace, Algorithm 1 is adopted, where three expansion points, i.e. $[k_{\mathrm{lef}}, k_{\mathrm{mid}}, k_{\mathrm{rig}}] = 2\pi \times [250, 500, 750]/c$ are designated to perform the SOAR algorithm. The associated maximum order $2\hat{M}$ of reduction basis corresponding to each $k_{\star}$ is also controlled by Eq. (14), which leads to $2\hat{M} = 42$ for case 1 and $2\hat{M} = 36$ for case 2.

Fig. 3 shows the variation of the condition number of the upper Hessenberg matrix $\hat{\mathbf{T}}$ with respect to the number of reduced order. It is obvious that the condition number quickly grows from 1 to the set maximum allowed value $\mathcal{O}(10^5)$ $(= \mathrm{lub}/\varepsilon)$ for case 1 and to $\mathcal{O}(10^4)$ for case 2, which verifies the premise of the adaptive process. Note that in Algorithm 1 looping j times will get $j+1$ columns of orthonormal basis vectors since the first vector $\mathbf{r}_0$ is given before iteration. Specifically, for case 1, the orthonormal basis with order $n = 82$ is obtained under a certain tolerance $\varepsilon = 0.01$, which consists of $n_{\mathrm{lef}} = 18$ for expansion point k_{lef}, $n_{\mathrm{mid}} = 23$ for k_{mid} and $n_{\mathrm{rig}} = 41$ for k_{rig}. From Fig. 3(a), it clearly indicates that as the frequency f (or wavenumber k) increases larger dimensions are required to enrich the projection subspace. A similar trend is observed for case 2 from Fig. 3(b), where the order $n = 61$ of the final reduced model is the sum of $n_{\mathrm{lef}} = 12$ for k_{lef}, $n_{\mathrm{mid}} = 21$ for k_{mid} and $n_{\mathrm{rig}} = 28$ for k_{rig}. This

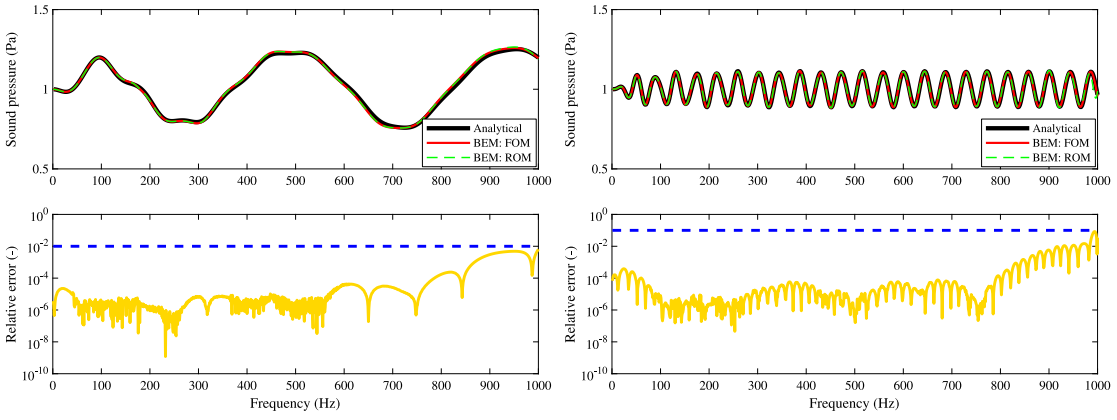

Fig. 4. Sound pressure responses and relative error between the FOM and ROM: (a) case 1 at ($r = 2R$, $\theta = \pi/2$) with $\varepsilon = 0.01$; (b) case 2 at ($r = 5R$, $\theta = \pi$) with $\varepsilon = 0.1$.

is due to the fact that more modal information is included in the higher frequency range, where more orthonormal vectors are subsequently required to capture the crucial dynamical characteristics of the original system.

Fig. 4 depicts the comparison of the obtained results between the original system of order $N = 2700$ and the reduced-order systems of order $n = 82$ for case 1 and $n = 61$ for case 2, together with the analytical solution obtained from Eq. (35) which serves as a reference. It can be intuitively seen that the BEM with the Burton–Miller formulation does not show any irregular modes, and the results are in agreement with the analytical solutions, which confirms the validity of the choice of $\beta = \mathrm{j}h$. In addition, the true relative error between the FOM and ROM is respectively shown at the second plot of Figs. 4(a) and 4(b), in which the blue dashed line indicates the set termination tolerance of ε. It is clear that the true relative error is less than ε over a wide frequency range, which implies that the dimension of ROM required for convergence can be automatically determined via the proposed adaptive process. It also suggests that the use of condition number of the upper Hessenberg matrix $\hat{\mathbf{T}}$ as an indicator is a good and cheap stopping criterion, which allows one to avoid excessive and wasteful iterations.

The elapsed time for obtaining the frequency response of the BE FOM is around 17.2 h. The total CPU time of the proposed AT-SOAR approach for case 1 is about 10 min, of which the processing time for the offline-phase and online-phase accounts for 95.7% and 4.3%, respectively. Excellent speedups over the brute force approach – of the order of 103 – are achieved, meanwhile keeping the relative error below 1% in the entire frequency range of interest. For case 2, the computing time of the present approach is 9 min. Therefore, the computational efficiency of frequency sweep analysis for BE models is significantly improved via the MOR technique.

With the obtained ROM, the sound field characteristics at any other field point in the exterior domain can be evaluated. For example, the directivity pattern of the (real and imaginary parts of) scattered pressure p^{S} is plotted in Fig. 5(a) at a radial distance of 10 m with azimuthal angle from 0 to 360° in the xy-plane, under a frequency of 200 Hz. Fig. 5(b) shows a polar plot of the scattered quantity at the points along a circle of radius 5 m with a frequency of 800 Hz. It is obvious that the present results obtained from the ROM are in excellent agreement with the analytical solutions. In addition, the scattering pattern becomes complicated as frequency increases.

5.2. Scattering from a soft sphere

The main objectives of this numerical case are to validate the proposed AT-SOAR technique for BE systems with the Dirichlet BC and to evaluate the results obtained from the present approach and the first-order Arnoldi-based (FOAR) process, which generates n number of column orthonormal vectors of the standard Krylov subspace $\mathcal{K}_n(\mathbf{C}, \mathbf{r}_0)$ [24,25]. A basic algorithm template is given in the Appendix, from which it is clear that the classical Krylov subspace-based method is a special case of the SOAR algorithm without the second-order term.

This example is equal to the previous one except that the plane wave propagating in the $+x$ direction is scattered by a soft sphere with zero surface pressure. The analytical solution for the total sound pressure at any field point

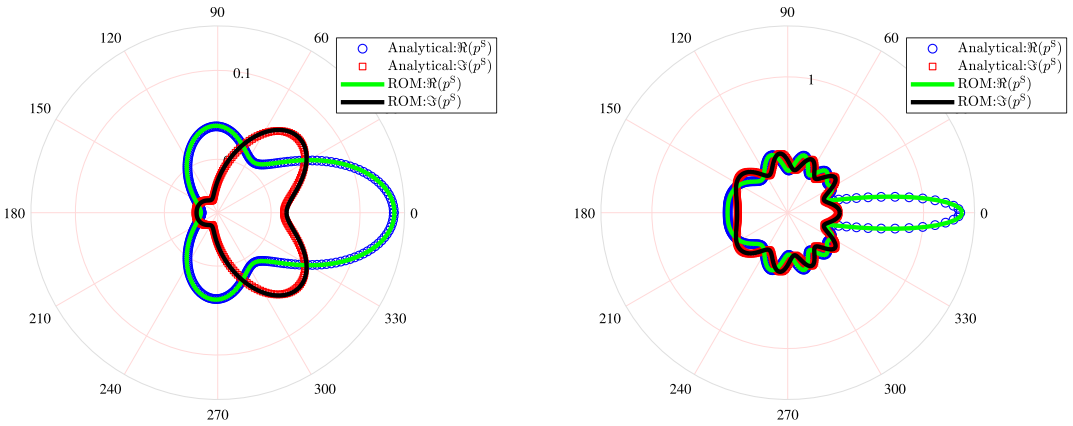

Fig. 5. Scattering directivity patterns versus the polar angle: (a) along a circle of radius 10 m at $f = 200$ Hz and (b) along a circle of radius 5 m at $f = 800$ Hz.

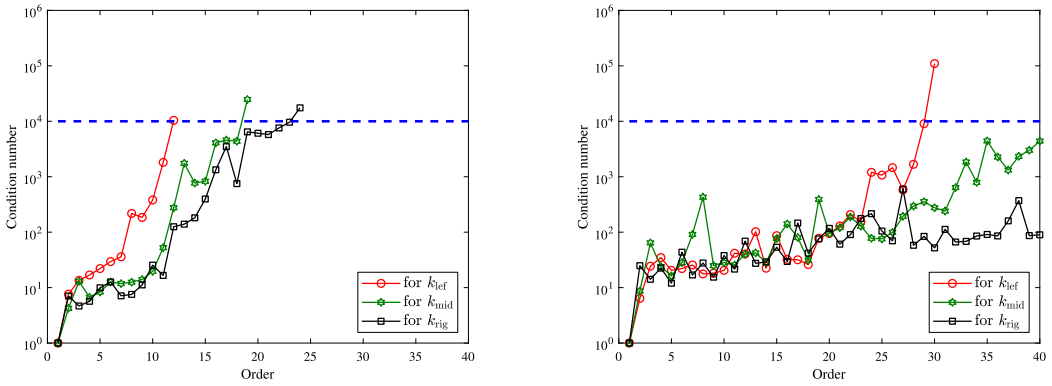

Fig. 6. Condition number of $\hat{\mathbf{T}}$ versus the order: (a) 1∼1000 Hz; (b) 1001∼2000 Hz.

is given by [49]

$$p(r,\theta) = \sum_{l=0}^{\infty} \mathrm{j}^l (2l+1) j_l(kr) P_l(\cos\theta) - \sum_{l=0}^{\infty} \mathrm{j}^l (2l+1) \frac{j_l(kR)}{h_l(kR)} h_l(kr) P_l(\cos\theta). \tag{36}$$

This time, the considered frequency band is enlarged from $f_{\min} = 1$ Hz to $f_{\max} = 2000$ Hz with 1 Hz increment, thus the required elements for the surface discretization is increased to 5808, which also means that the order of this system is $N = 5808$. The total sound pressure distributions induced by the incident wave at the field point ($r = 2R$, $\theta = \pi/2$) and ($r = 5R$, $\theta = \pi$) with prescribed threshold $\varepsilon = 0.1$ are reported. The partition of the considered frequency range is conducted, where the first subinterval is from 1 Hz to 1000 Hz with the expansion point $k_\circ = 2\pi \times 500/c$. The second one is from 1001 Hz to 2000 Hz with $k_\circ = 2\pi \times 1500/c$.

Fig. 6 shows how the condition number of $\hat{\mathbf{T}}$ varies with the change of order $n_\star$. For the first frequency sub-range, a reduced model with $n = 58$ is generated, which is the sum of $n_{\text{lef}} = 13$, $n_{\text{mid}} = 20$ and $n_{\text{rig}} = 25$. For the second one, a reduced model with $n = 113$ is created from the combination of $n_{\text{lef}} = 31$, $n_{\text{mid}} = 41$ and $n_{\text{rig}} = 41$. For $f_{\text{mid}} = 1500$ Hz and $f_{\text{rig}} = 1750$ Hz, it is obvious from Fig. 6(b) that the maximum condition number of $\hat{\mathbf{T}}$ is below $\mathcal{O}(10^4)$ and their orders are controlled by the setting of the supremum of order $2\hat{M}$. In this situation, the pressure frequency spectrum of reduced model still approximates that of the original model very well, as can be seen in Fig. 8, thereby highlighting the rationality of the $2\hat{M}$ setting.

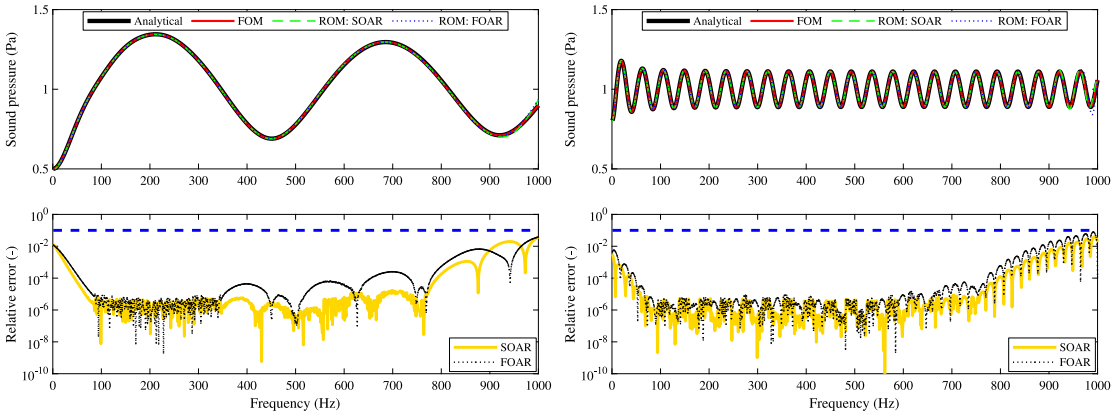

(a) (b)

Fig. 7. Sound pressure responses and relative errors between the FOM and ROMs over 1∼1000 Hz with $\varepsilon = 0.1$: (a) at ($r = 2R$, $\theta = \pi/2$); (b) at ($r = 5R$, $\theta = \pi$).

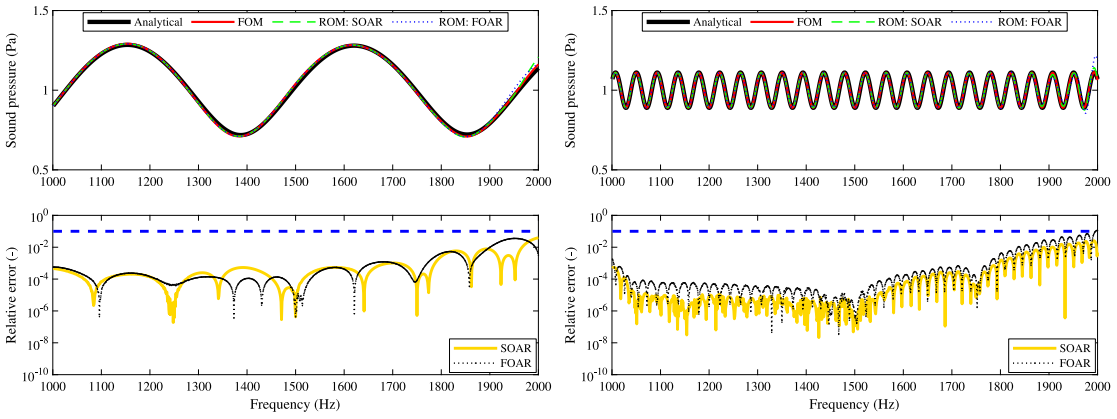

(a) (b)

Fig. 8. Sound pressure responses and relative errors between the FOM and ROMs over 1001∼2000 Hz with $\varepsilon = 0.1$: (a) at ($r = 2R$, $\theta = \pi/2$); (b) at ($r = 5R$, $\theta = \pi$).

The computed results of the original system of order $N = 5808$ and the reduced-order systems of order $n = 58$ for the former frequency interval and $n = 113$ for the latter one, along with the analytical solutions are respectively illustrated in Figs. 7 and 8. As the plots show, the present solutions are very close to the analytical and reference FOM results. Once again, the proposed adaptive process provides a cheap tool to ensure adequate accuracy for frequency sweep analyses of BE systems, and hence it is a suitable and achievable convergence criterion. In addition, these results together with the previous ones from Section 5.1 demonstrate that a relatively wide frequency band can be divided into several sub-ranges, within each range a single expansion point can be allocated and to the end its multi-point counterparts covering the entire frequency band are formed. Furthermore, different element sizes (and number of meshes) can be applied for different frequency sub-ranges according to the rule of thumb.

For the purpose of comparisons, we include the results obtained from the standard Arnoldi-based algorithm with the same expansion points $k_\circ$ and the same reduced order n. It is evident from Figs. 7 and 8 that the present AT-SOAR approach is more accurate than the FOAR for the dimension reduction of BE systems formed by the Burton–Miller BIE formulation.

In this verification case, the CPU time required to solve the FOM at 1000 frequency points is about 76.9 h. The total simulation time of the present approach is 36 min for the first frequency range and 38 min for the second one. Specifically, the largest proportion of the execution time happens in the offline phase (98.0%) and the online

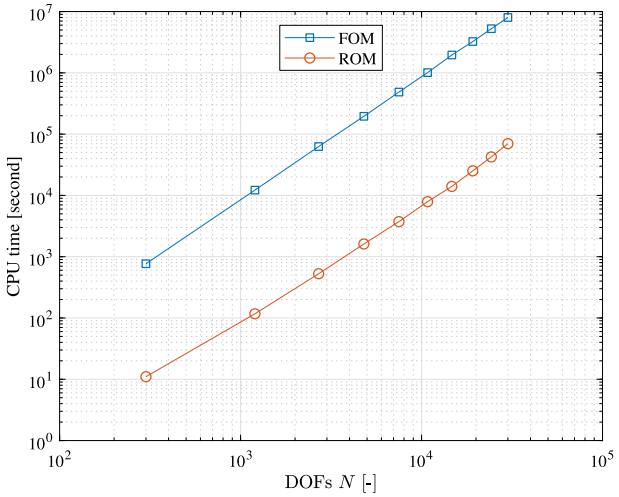

Fig. 9. CPU time with respect to the number of DOFs N of the FOM.

frequency sweep analysis is fast (less than 1 min) since only low-dimensional approximated model rather than the original model needs to be confronted. The computational merit of the proposed AT-SOAR approach is apparent with a speed-up ratio of about 121 times. If only the online frequency sweep operation is assessed, this merit is even more pronounced by a factor of more than 6000.

In order to further investigate the computational efficiency of the proposed methodology, a comparison analysis is performed. Fig. 9 shows the variation of the total CPU time as a function of the number of order N (DOFs of the FOM), where the sphere surface is meshed from coarse- to high-resolution discretization. It clearly indicates that the present MOR technique is beyond two orders of magnitude faster than the directly computed FOM counterpart.

5.3. Scattering from a skipjack-class submarine model

For the last numerical example, we consider a complex skipjack-class submarine model, which is downloaded from 3D CAD Browser [50] and graphically shown in Fig. 10. The submarine's outer bounding box has dimensions $76.81 \times 17.36 \times 10.67$ m and it is discretized using 26 649 constant triangular elements with 13 782 vertices. The structure is immersed in an infinite extent filled with water and it is assumed to have a sound-hard surface. The incident field is coming from a plane wave with a unit amplitude traveling in the direction $(1, -1, -1)$. The purpose of this case study is to assess the performance and robustness of the proposed AT-SOAR method for a complex industrial geometry.

The frequency is swept over the band 0.5∼200 Hz in a 0.5 Hz increment because of rapidly varying responses in the far-field. The expansion point $k_\circ$ is placed in the middle of the frequency range, i.e. $k_\circ = 2\pi \times 100/c$. As mentioned before, Eq. (14) provides an estimator for the error originating from the Taylor series truncation. For this case, the maximum distance r_d of two points on the submerged structure is its length of 76.81 m, thus $M = 82$ is required to satisfy the set tolerance $\varepsilon = 0.1$ across the entire frequency range. Three expansion points, i.e. $k_\mathrm{lef} = 2\pi \times 50/c$, $k_\mathrm{mid} = 2\pi \times 100/c$ and $k_\mathrm{rig} = 2\pi \times 150/c$ are employed to generate a global frequency-independent orthonormal basis. Due to the presence of large-size structure, $4\hat{M} = 160$ for each expansion point is set.

Fig. 11 shows the absolute sound pressure responses of the FOM with $N = 26649$ and the ROM with $n = 483$ at three different field points, i.e. (350, 0, 0) m, (−350, 0, 0) m and (0, 350, 0) m. The errors between the FOM and ROM are not given herein due to the relatively small changes in amplitude. The variation with the frequency of the total sound pressure $|p(r, \theta)|$ located in the far-field is rapid, especially on the back of scatterers. The same behavior can also be observed from the previous two verification cases. Once again, the transfer function of the ROM approximates that of the FOM very well.

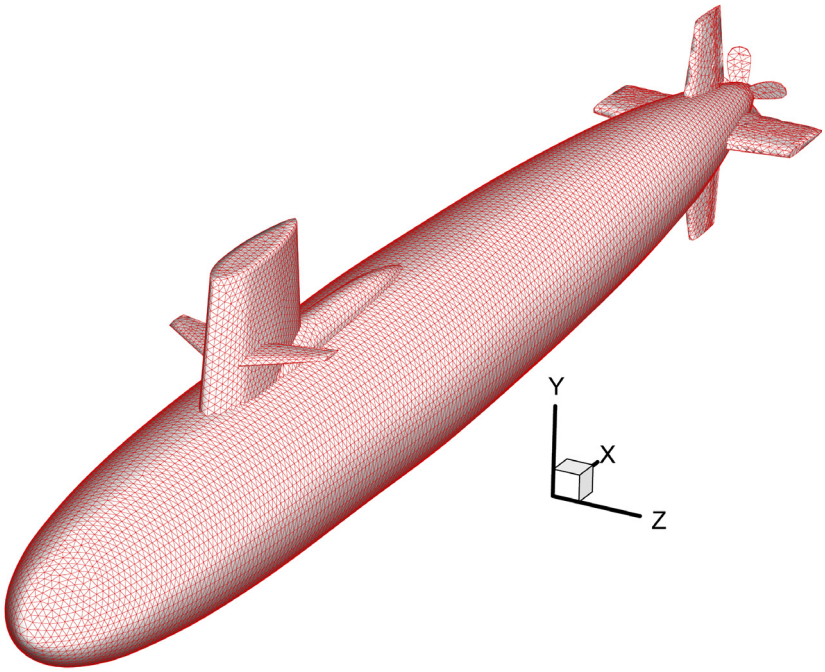

Fig. 10. The considered skipjack-class submarine model and its BE mesh.

The real parts of sound pressure field $\Re(p)$ of the FOM and ROM at four different frequencies of 50, 100, 150 and 200 Hz are compared in Fig. 12. It is obvious that the constructed ROM accurately predicts the surface pressure p at all the BE independent DOFs.

For this case, the computational time required for solving the FOM is 707 h. The CPU time required for the proposed AT-SOAR method is 37.1 h, in which the offline phase takes up the largest percentage (99.9%) whereas the elapsed time needed for the online phase that is to perform the simulation of the ROM can be negligible (only 0.1%). Therefore, the present adaptive MOR technique is a good way to obtain reliable solution with an acceptable CPU time.

6. Conclusions

This paper proposes an efficient offline–online computational strategy for the acceleration of frequency sweep analysis of exterior acoustic problems with different boundary conditions. The Burton–Miller BIE formulation is used to deal with the fictitious eigenfrequency difficulty. The proposed model order reduction technique, AT-SOAR in short, is first based on a frequency affine decomposition of the frequency-dependent property of the integral kernels, where a local Taylor approximation is utilized; then followed by the SOAR algorithm to generate a frequency-independent orthonormal reduction basis. A simple, cheap yet efficient adaptive scheme based on the condition number of the upper Hessenberg matrix in the SOAR is further provided such that the dimension of reduced system required for the desired accuracy can be determined before the congruence transformations start. This way the computation of the FOM, comparison between different ROMs and unnecessary iterations can be avoided. The frequency-independent reduction basis is then leveraged in the projection of the full-order, frequency-decoupled system matrices, where a column-by-column projection is done to favorably handle the memory problem caused by the series expansion. The comparison between the present AT-SOAR and the Krylov subspace-based Arnoldi procedure is conducted and the suggestion on the multi-point expansions for relatively high-frequency range and large-size structures is given. We have verified the simplicity and high-efficiency of the proposed overall strategy in terms of both decreased DOFs and runtime.

The established solution framework can be directly combined with the BEM to perform high-fidelity and broadband multi-frequency analyses of increasingly complex systems in such a way that numerical simulation (of

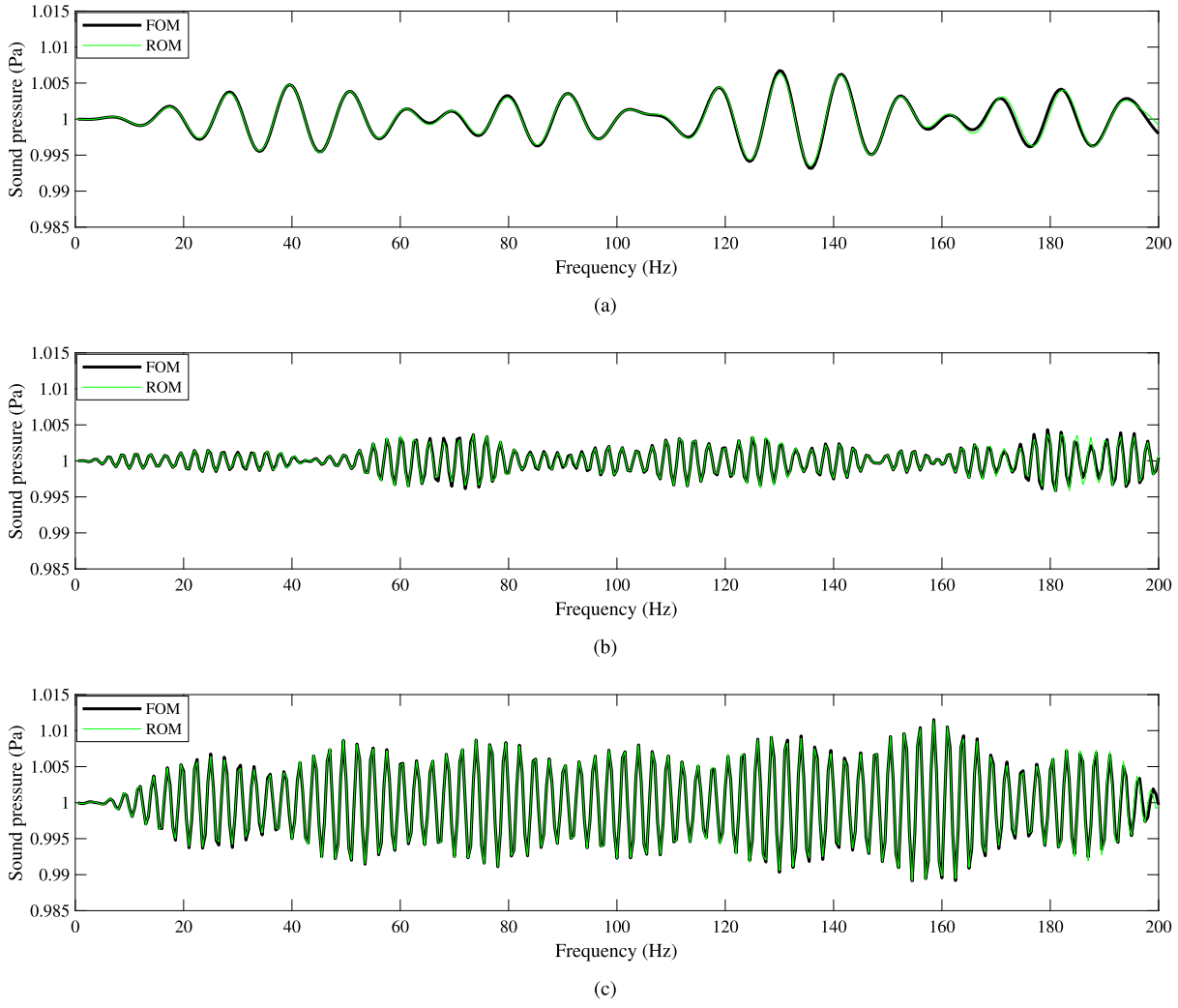

Fig. 11. Comparison of sound pressure responses between the FOM and ROM: (a) at point (350, 0, 0) m; (b) at point (−350, 0, 0) m and (c) at point (0, 350, 0) m.

noise control and low-noise design) demands can be significantly reduced. In view of engineering sound-structure interaction environment, it would be worthwhile to further extend present approach to vibro-acoustic coupling problems. Another important extension of this work is the combination of the fast multipole BEM and MOR technique, where one uses far-field multipole and local expansions to manage the space domain and one uses e.g. Taylor expansion to separate the frequency domain.

Declaration of competing interest

The authors declare that they have no known competing financial interests or personal relationships that could have appeared to influence the work reported in this paper.

Acknowledgments

The authors would like to acknowledge the funding support from the National Natural Science Foundation of China (Grant No. 12002146 and No. 11972179). The research of X. Xie is also funded by the China Postdoctoral Science Foundation (Project No. 2020M672696).

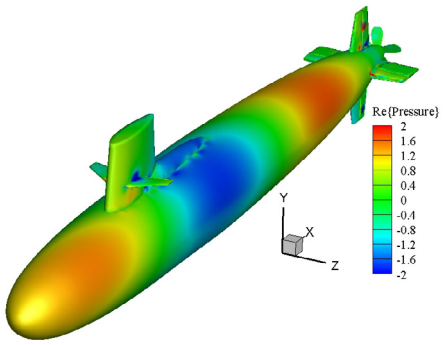

(a) FOM at $f = 50$ Hz

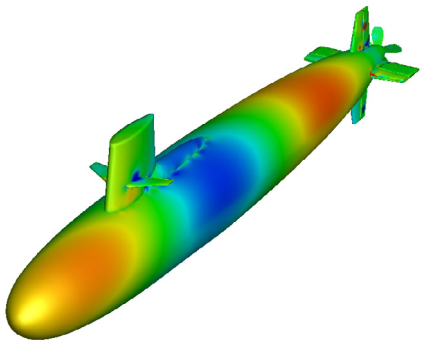

(b) ROM at $f = 50$ Hz

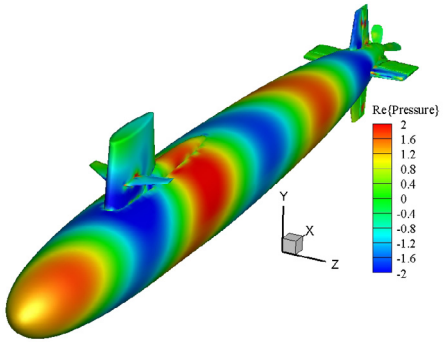

(c) FOM at $f = 100$ Hz

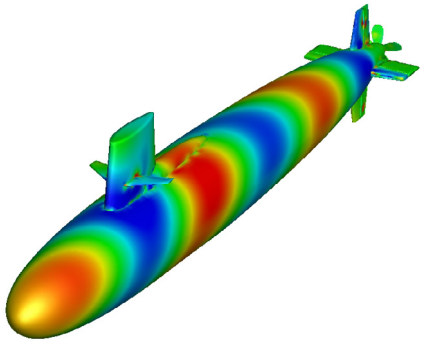

(d) ROM at $f = 100$ Hz

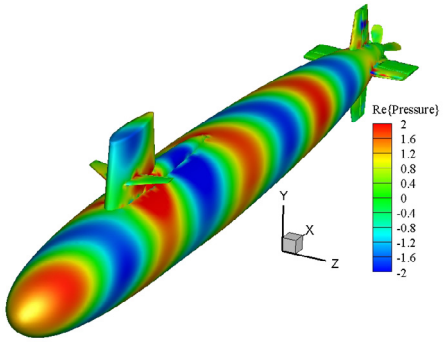

(e) FOM at $f = 150$ Hz

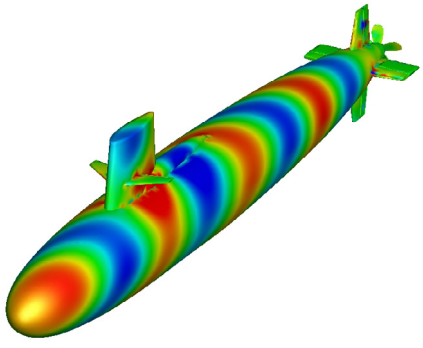

(f) ROM at $f = 150$ Hz

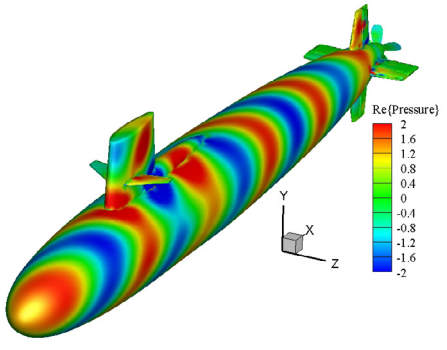

(g) FOM at $f = 200$ Hz

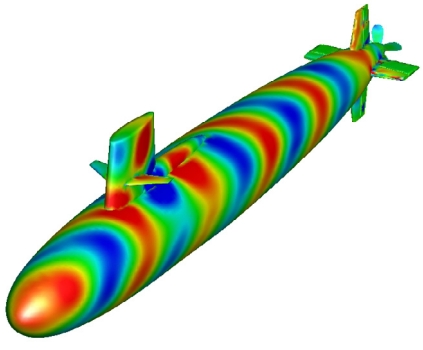

(h) ROM at $f = 200$ Hz

Fig. 12. Real parts of sound pressure distributions of the FOM (left) and ROM (right) at different frequencies.

Appendix. The Arnoldi-based Krylov subspace technique

Algorithm 4 Algorithm template for the Arnoldi process

Input: $\mathbf{C}$, $\mathbf{r}_0$; **Output:** $\mathbf{Q}_\star$ for selected $k_\star$ with $\star$ being [lef, mid, rig]

preallocate $\mathbf{Q} = \text{zeros}(N, 2\hat{M}+1)$
$\mathbf{q}_1 = \mathbf{r}_0/\|\mathbf{r}_0\|_2$
for $j = 1, 2, \cdots, 2\hat{M}$ **do**
  $\mathbf{r} = \mathbf{C}\mathbf{q}_j$
  for $i = 1, 2, \cdots, j$ **do**
    $t_{ij} = \mathbf{q}_i^{\mathrm{H}}\mathbf{r}$
    $\mathbf{r} = \mathbf{r} - \mathbf{q}_i t_{ij}$
  end for
  $t_{j+1,j} = \|\mathbf{r}\|_2$
  if $t_{j+1,j} \neq 0$ **then**
    $\mathbf{q}_{j+1} = \mathbf{r}/t_{j+1,j}$
  else
    breakdown
  end if
end for
$\mathbf{Q}_\star = \mathbf{Q}_{j+1}$

Notations: $\mathbf{C} = -(\mathbf{W}_0 + k_\star\mathbf{V}_0)^{-1}\mathbf{V}_0$, $\mathbf{r}_0 = (\mathbf{W}_0 + k_\star\mathbf{V}_0)^{-1}\mathbf{b}_{\mathrm{p}}$.

References

[1] O. Zienkiewicz, R. Taylor, J. Zhu, Finite element method - its basis and fundamentals, in: O. Zienkiewicz, R. Taylor, J. Zhu (Eds.), Elservier, sixth ed., Elsevier, London, 2005, pp. 1–749.
[2] C.A. Brebbia, The Boundary Element Method for Engineers, Pentech Press, 1978, pp. 1–189.
[3] H.A. Schenck, Improved integral formulation for acoustic radiation problems, J. Acoust. Soc. Am. 44 (1) (1968) 41–58.
[4] A.J. Burton, G.F. Miller, The application of integral equation methods to the numerical solution of some exterior boundary-value problems, Proc. R. Soc. Lond. Ser. A Math. Phys. Eng. Sci. 323 (1553) (1971) 201–210.
[5] S. Amini, P.J. Harris, A comparison between various boundary integral formulations of the exterior acoustic problem, Comput. Methods Appl. Mech. Engrg. 84 (1) (1990) 59–75.
[6] Y.J. Liu, On the BEM for acoustic wave problems, Eng. Anal. Bound. Elem. 107 (2019) 53–62.
[7] N. Nishimura, Fast multipole accelerated boundary integral equation methods, Appl. Mech. Rev. 55 (4) (2002) 299–324.
[8] Y.J. Liu, Fast Multipole Boundary Element Method: Theory and Applications in Engineering, Cambridge University Press, 2009, pp. 1–235.
[9] N. Kamiya, E. Andoh, K. Nogae, Eigenvalue analysis by the boundary element method: new developments, Eng. Anal. Bound. Elem. 12 (3) (1993) 151–162.
[10] A. Ali, C. Rajakumar, S.M. Yunus, Advances in acoustic eigenvalue analysis using boundary element method, Comput. Struct. 56 (5) (1995) 837–847.
[11] C.J. Zheng, H.F. Gao, L. Du, H.B. Chen, C. Zhang, An accurate and efficient acoustic eigensolver based on a fast multipole BEM and a contour integral method, J. Comput. Phys. 305 (2016) 677–699.
[12] J. Xiao, S. Meng, C. Zhang, C. Zheng, Resolvent sampling based Rayleigh–Ritz method for large-scale nonlinear eigenvalue problems, Comput. Methods Appl. Mech. Engrg. 310 (2016) 33–57.
[13] S. Li, An efficient technique for multi-frequency acoustic analysis by boundary element method, J. Sound Vib. 283 (3–5) (2005) 971–980.
[14] Z. Wang, Z.G. Zhao, Z.X. Liu, Q.B. Huang, A method for multi-frequency calculation of boundary integral equation in acoustics based on series expansion, Appl. Acoust. 70 (3) (2009) 459–468.
[15] Q. Zhang, Y. Mao, D. Qi, Y. Gu, An improved series expansion method to accelerate the multi-frequency acoustic radiation prediction, J. Comput. Acoust. 23 (1) (2015).
[16] Y. Shi, X. Chen, Y. Tan, H. Jiang, S. Liu, Reduced-basis boundary element method for fast electromagnetic field computation, J. Opt. Soc. Amer. A 34 (12) (2017) 2231–2242.
[17] U. Hetmaniuk, R. Tezaur, C. Farhat, Review and assessment of interpolatory model order reduction methods for frequency response structural dynamics and acoustics problems, Int. J. Numer. Methods Eng. 90 (13) (2012) 1636–1662.
[18] S.T. Raveendra, An efficient indirect boundary element technique for multi-frequency acoustic analysis, Internat. J. Numer. Methods Engrg. 44 (1) (1999) 59–76.

[19] O. Von Estorff, O. Zaleski, Efficient acoustic calculations by the BEM and frequency interpolated transfer functions, Eng. Anal. Bound. Elem. 27 (7) (2003) 683–694.
[20] S. Lefteriu, M. Souza Lenzi, H. Bériot, M. Tournour, W. Desmet, Fast frequency sweep method for indirect boundary element models arising in acoustics, Eng. Anal. Bound. Elem. 69 (2016) 32–45.
[21] D. Ryckelynck, L. Hermanns, F. Chinesta, E. Alarcón, An efficient 'a priori' model reduction for boundary element models, Eng. Anal. Bound. Elem. 29 (8) (2005) 796–801.
[22] H. Jiang, X. Zhang, X. Huang, Reduced-basis boundary element method for efficient broadband acoustic simulation, J. Sound Vib. 456 (2019) 374–385.
[23] S.K. Baydoun, M. Voigt, C. Jelich, S. Marburg, A greedy reduced basis scheme for multifrequency solution of structural acoustic systems, Internat. J. Numer. Methods Engrg. 121 (2) (2020) 187–200.
[24] E.J. Grimme, Krylov projection methods for model reduction, in: Vasa (Ph.D. thesis), University of Illinois at Urbana-Champaign, 1997.
[25] Z. Bai, Krylov subspace techniques for reduced-order modeling of large-scale dynamical systems, Appl. Numer. Math. 43 (1–2) (2002) 9–44.
[26] A.C. Antoulas, Approximation of Large-Scale Dynamical Systems, Society for Industrial and Applied Mathematics, 2005.
[27] S. Keuchel, J. Biermann, O. Von Estorff, A combination of the fast multipole boundary element method and Krylov subspace recycling solvers, Eng. Anal. Bound. Elem. 65 (2016) 136–146.
[28] X. Xie, H. Zheng, S. Jonckheere, A. van de Walle, B. Pluymers, W. Desmet, Adaptive model reduction technique for large-scale dynamical systems with frequency-dependent damping, Comput. Methods Appl. Mech. Engrg. 332 (2018) 363–381.
[29] X. Xie, H. Zheng, S. Jonckheere, W. Desmet, Acoustic simulation of cavities with porous materials using an adaptive model order reduction technique, J. Sound Vib. 485 (2020) 115570.
[30] D. Panagiotopoulos, E. Deckers, W. Desmet, Krylov subspaces recycling based model order reduction for acoustic BEM systems and an error estimator, Comput. Methods Appl. Mech. Engrg. 359 (2020) 112755.
[31] Z. Bai, Y. Su, SOAR: A second-order Arnoldi method for the solution of the quadratic eigenvalue problem, SIAM J. Matrix Anal. Appl. 26 (3) (2005) 640–659.
[32] J. Jith, S. Sarkar, A model order reduction technique for systems with nonlinear frequency dependent damping, Appl. Math. Model. 77 (2020) 1662–1678.
[33] R. Srinivasan Puri, D. Morrey, A.J. Bell, J.F. Durodola, E.B. Rudnyi, J.G. Korvink, Reduced order fully coupled structural-acoustic analysis via implicit moment matching, Appl. Math. Model. 33 (11) (2009) 4097–4119.
[34] X. Xie, H. Zheng, S. Jonckheere, B. Pluymers, W. Desmet, A parametric model order reduction technique for inverse viscoelastic material identification, Comput. Struct. 212 (2019) 188–198.
[35] X. Xie, H. Zheng, S. Jonckheere, W. Desmet, Explicit and efficient topology optimization of frequency-dependent damping patches using moving morphable components and reduced-order models, Comput. Methods Appl. Mech. Engrg. 355 (2019) 591–613.
[36] C.J. Zheng, H.B. Chen, H.F. Gao, L. Du, Is the Burton–Miller formulation really free of fictitious eigenfrequencies? Eng. Anal. Bound. Elem. 59 (2015) 43–51.
[37] S. Marburg, The burton and miller method: Unlocking another mystery of its coupling parameter, J. Comput. Acoust. 24 (1) (2016).
[38] Y.J. Liu, F.J. Rizzo, A weakly singular form of the hypersingular boundary integral equation applied to 3-D acoustic wave problems, Comput. Methods Appl. Mech. Engrg. 96 (2) (1992) 271–287.
[39] M. Guiggiani, G. Krishnasamy, T.J. Rudolphi, F.J. Rizzo, A general algorithm for the numerical solution of hypersingular boundary integral equations, J. Appl. Mech. Trans. ASME 59 (3) (1992) 604–614.
[40] G. Karami, D. Derakhshan, An efficient method to evaluate hypersingular and supersingular integrals in boundary integral equations analysis, Eng. Anal. Bound. Elem. 23 (4) (1999) 317–326.
[41] X.W. Gao, An effective method for numerical evaluation of general 2D and 3D high order singular boundary integrals, Comput. Methods Appl. Mech. Engrg. 199 (45–48) (2010) 2856–2864.
[42] R.N. Simpson, M.A. Scott, M. Taus, D.C. Thomas, H. Lian, Acoustic isogeometric boundary element analysis, Comput. Methods Appl. Mech. Engrg. 269 (2014) 265–290.
[43] L.L. Chen, H. Lian, Z. Liu, H.B. Chen, E. Atroshchenko, S.P. Bordas, Structural shape optimization of three dimensional acoustic problems with isogeometric boundary element methods, Comput. Methods Appl. Mech. Engrg. 355 (2019) 926–951.
[44] S.M. Kirkup, S. Amini, Solution of the Helmholtz eigenvalue problem via the boundary element method, Internat. J. Numer. Methods Engrg. 36 (2) (1993) 321–330.
[45] Z. Bai, Y. Su, Dimension reduction of large-scale second-order dynamical systems via a second-order Arnoldi method, SIAM J. Sci. Comput. 26 (5) (2005) 1692–1709.
[46] D. Lu, Y. Su, Z. Bai, Stability analysis of the two-level orthogonal Arnoldi procedure, SIAM J. Matrix Anal. Appl. 37 (1) (2016) 195–214.
[47] A. Salvadori, Analytical integrations of hypersingular kernel in 3D BEM problems, Comput. Methods Appl. Mech. Engrg. 190 (31) (2001) 3957–3975.
[48] F. Ihlenburg, Finite Element Analysis of Acoustic Scattering, Springer, 1998, pp. 1–224.
[49] S. Turley, Acoustic Scattering from a Sphere, Tech. Rep., 2006.
[50] 3D CAD Browser. URL https://www.3dcadbrowser.com/.